THE ASTROPHYSICAL JOURNAL, 389:157–178, 1992 April 10

THE X-RAY SPECTRA OF HIGH-LUMINOSITY ACTIVE GALACTIC NUCLEI OBSERVED BY *GINGA*

O. R. WILLIAMS,[1] M. J. L. TURNER, G. C. STEWART, AND R. D. SAXTON
Department of Physics and Astronomy, University of Leicester, University Road, Leicester LE1 7RH, UK

T. OHASHI AND K. MAKISHIMA
Department of Physics, University of Tokyo, 7-3-1, Hongo, Bunkyo-ku, Tokyo 113, Japan

T. KII, H. INOUE, AND F. MAKINO
Institute of Space and Astronautical Science, 3-1-1, Yoshinodai, Sagamihara, Kanagawa 229, Japan

K. HAYASHIDA
Department of Earth and Space Science, Faculty of Science, Osaka University,
1-1 Machikaneyama-cho, Toyonaka, Osaka 560, Japan

AND

K. KOYAMA
Department of Physics, Kyoto University, Sakyo-ku, Kyoto 606-01, Japan
Received 1991 February 8; accepted 1991 October 7

ABSTRACT

Results are presented on the X-ray emission from 13 objects, observed by *Ginga* as part of a spectral survey of bright quasars in the energy range 2–20 keV. The distribution of the power-law energy index for this sample has a mean of $\bar{\alpha} = 0.81$ and shows significant intrinsic dispersion, $\sigma = 0.31$, values which are broadly compatible with those from samples of lower luminosity active galactic nuclei. The mean spectral slope is clearly too steep to fit the spectrum of the cosmic diffuse X-ray background (CXB) at energies less than 20 keV, confirming the "spectral paradox" in the discrete-source explanation of the CXB. We have searched for correlations between the X-ray spectral properties and those in other frequency bands, and have found a possible connection between the near-infrared spectral indices and the X-ray properties of quasars. There is also evidence that quasars with steep X-ray spectra are radio-quiet, in support of the previous results obtained for the 0.3–3.5 keV band; our results, however, are compatible with a single power-law component in the 0.3–10 keV range, in contrast to some previous results. The first evidence for departures from a simple power-law continuum in Mrk 205 is revealed; this, together with previously reported evidence for iron lines in other quasars, suggests that an appreciable fraction of quasars may possess iron lines with equivalent widths ~ 100 eV. Models involving reprocessing of continuum flux in cool material near the core, successful in the case of Seyfert galaxies, fit well for the lower luminosity objects in our sample; for the high-luminosity objects the fit is not as good, and other processes, such as beaming, may be implicated.

Subject headings: galaxies: active — galaxies: nuclei — quasars: general — X-rays: galaxies

1. INTRODUCTION

This paper reports the study, made with *Ginga*, of the X-ray spectra of quasars; the term "quasar" refers, in this paper, to high-luminosity, unpolarized, active galactic nuclei (AGNs). The large area counter (LAC) on *Ginga* is the first instrument capable of measuring the spectrum of a significant number of quasars in the 2–10 keV band with reasonable accuracy. The X-ray emission of AGNs is important: the rapid variability seen in Seyfert galaxies (see McHardy 1989 for a recent review) indicates that its origin is within a few hundred astronomical units of the core. It can thus be expected to yield information on the conditions in the core, and the mechanisms producing the AGN continuum. The form of the X-ray continuum of quasars has been the subject of a number of studies in the energy range 0.3–3.5 keV using data from the *Einstein Observatory*; however, it has been difficult to measure quasar X-ray continua above the upper energy limit of the *Einstein Observatory*, because of the lack of sensitive instruments. The 2–10 keV spectrum of quasars is of particular interest for two reasons: to establish whether quasars have continua similar to those of Seyfert galaxies, which might indicate that similar mechanisms pertain to the AGN phenomenon over the full range of luminosities; and to establish the level at which quasars may contribute to the diffuse cosmic X-ray background (CXB). Here the form of the continuum at high redshifts is vital, since there is a discrepancy between the spectral index of low-redshift AGNs and the CXB: below 40 keV the effective index of the CXB is ~ 0.4, while Seyfert galaxies and BL Lacertae objects have indices ~ 0.7 and ~ 1.0, respectively.

The studies of the soft, 0.3–3.5 keV X-ray continua of quasars with *Einstein* have revealed significant information. The notable compilation by Wilkes & Elvis (1987) contained spectra from 33 quasars with redshifts from ~ 0.05 to ~ 1.0. They found a wide spread ($0.3 \leq \alpha \leq 1.8$) in the power-law index measured in the *Einstein* band, in contrast to the tighter grouping of the 2–10 keV spectra of lower luminosity AGNs (e.g., Turner & Pounds 1989), and also found a correlation between radio-loudness and hard X-ray spectra. One possible explanation for this is that there are two distinct classes of quasars, radio-loud and radio-quiet; an alternative explanation, suggested by Wilkes & Elvis, is that quasar 0.3–3.5 keV

[1] Postal address: Serco, ESTEC, Keplerlaan 1, Noordwijk, The Netherlands.

spectra consist of several components with differing spectral characteristics, one of which has a relatively flat slope ($\alpha \sim 0.5$) and is linked to the radio emission. Subsequent studies using a large sample of *Einstein* quasars have broadly confirmed the results of Wilkes & Elvis: Canizares & White (1989) found that flat radio spectrum (FRS) quasars have $\alpha \sim 0.4$, steep radio spectrum (SRS) quasars have $\alpha \sim 0.7$, and radio-quiet (RQ) quasars have $\alpha \sim 1$–1.4; Worrall (1989) confirmed that flat X-ray spectra are associated with radio-loud (RL) quasars, but found that evidence for a difference between core-dominated FRS quasars and lobe-dominated SRS quasars was weak. The measurements of the spectral index in the higher energy range covered by *Ginga*, presented in this paper, will clearly be important in helping to distinguish the various possible components in the spectra of quasars.

It will be valuable to compare the 2–10 keV spectra of quasars measured by *Ginga* with those of lower luminosity AGNs: significant progress has been made in establishing the form of the X-ray continua of both polarized and unpolarized lower luminosity AGNs, BL Lacertae objects, and Seyfert galaxies, and on the relationship between their X-ray emission and their continua in other wave bands. BL Lac objects have simple spectra without emission lines or thermal bumps, allowing us to view the nonthermal emission which frequently takes the form of a continuously steepening continuum from the radio to X-ray. In some sources, however, the X-ray continuum lies above a smooth extension of the infrared to ultraviolet (IR–UV) synchrotron emission, and probably arises from another process, such as synchrotron–self-Compton (SSC) (e.g., Jones, O'Dell, & Stein 1974; Zdziarski 1986) pair cascade models (Fabian 1988), or Compton scattering of optical photons. In general there is a good correlation between the X-ray and radio flux levels of samples of blazars (Worrall 1988), a class which includes both BL Lac objects and optically violently variable (OVV) quasars; this may be viewed as support for the SSC model. However, this test is not conclusive, since there is typically a good flux level correlation among all wave bands, and only in a few cases (e.g., 3C 345; Bregman et al. 1986) do *variations* in the X-ray and radio flux of individual objects appear to be associated. The majority of Seyfert galaxies have power-law spectra in the band 2–10 keV with a spectral index, α, close to 0.7 (Turner & Pounds 1989), the existence of a common index for Seyferts perhaps being indicative of a common mechanism which may also apply to quasars. The similarity of the X-ray spectral index to that in the IR and (for radio-loud objects) radio suggests that these emission bands may have their origin in a common population of electrons via, for example, the SSC mechanism.

The low-energy (LE) experiment on *EXOSAT* showed that many Seyfert galaxies have soft X-ray emission in excess of that projected from a simple power law in the 2–10 keV band (e.g., Arnaud et al. 1985; Pounds et al. 1986), a feature that has commonly been attributed to the high-energy part of the "blue bump" associated with thermal emission from an accretion disk. If relatively cool material is present near the core of an AGN, it may also be expected to show itself by means of fluorescent and other features imprinted on the 2–10 keV continuum spectrum. Measurements of the 2–10 keV AGN spectra prior to the launch of *Ginga* showed that most were well fitted by simple power-law continua, but *Ginga* observations of Seyfert galaxies have revealed evidence, in the form of iron emission and absorption features, for cold material near the core (Pounds 1989; Piro, Matsuoka, & Yamauchi 1989; Matsuoka et al. 1986; Pounds et al. 1989). A consensus still has not been reached as to the form of such cold material: suggested geometries include an accretion disk and dense clouds covering part of the X-ray–emitting region (Pounds 1989; Pounds et al. 1989; Matsuoka et al. 1990). However, the simple presence of such material has wide-ranging consequences, not least of which is the expected flattening of the spectrum above 10 keV due to Compton scattering; this has obvious implications for the possible role of Seyfert galaxies and quasars as contributors to the CXB. Detailed studies on the two brightest objects in our sample, the radio-loud quasar 3C 273 (Turner et al. 1990) and the radio-quiet quasar E1821+643 (Kii et al. 1991) have established the presence of iron emission lines in the spectra of both sources, suggesting similarities in this respect between Seyfert I galaxies and quasars. A search for iron emission features and spectra flattening in the remainder of our sample of quasars is necessary to show whether such features are a common property of quasars.

In this paper we report on the spectral index and luminosity in the 2–10 keV band of 13 quasars, and search for correlations with the radio and IR bands. We also report on the search for deviations from a simple power continuum, particularly those, such as iron emission and absorption features or high-energy excesses ("hard tails"), which may indicate the presence of cold material near the quasar center. We compare our results with earlier 0.3–3.5 keV band measurements of quasars, and also with 2–10 keV band measurements of Seyfert galaxies. The impact of our measurements on the discrete-source explanation of the CXB is discussed.

2. OBSERVATIONS AND DATA ANALYSIS

The *Ginga* program of quasar observations plans to study systematically the brightest X-ray quasars (as measured in the *Einstein* band) listed in Hewitt & Burbidge (1987) with luminosities of $\sim 10^{44}$ ergs s^{-1} or greater. We do not include BL Lac and OVV quasars in this study, and so have excluded objects which also appear in the list of polarized sources in Angel & Stockman (1980).

The *Ginga* observations described in this paper were made between 1987 July and 1989 December. The bright quasar 3C 273 was observed 5 times as part of a campaign of multi–wave-band observations, the results of which are published in Courvoisier et al. (1990). A complete report on the X-ray emission of 3C 273 including *Ginga* and *EXOSAT* data has been given in Turner et al. (1990), and a study of E1821+643 appears in Kii et al. (1991). The other quasars were observed once each as part of the UK–Japan collaboration to observe bright, high-luminosity AGNs; the dates and details of the observations are given in Table 1. The LAC instrument is described in Turner et al. (1989), and the *Ginga* satellite is described in Makino et al. (1987). For present purposes, only data from the top layer (1.5–35 keV) were used; the total effective area is 4000 cm^2, and the energy resolution is 18% at 6 keV. *Ginga* is sensitive down to a flux level of $\sim 3 \times 10^{-12}$ ergs s^{-1} cm^{-2} in the 2–10 keV band (Hayashida et al. 1989); the measured fluxes from PG 1407+265 and PG 1352+183 (see Tables 2 and 3) fell below this limit and were excluded from the subsequent detailed analysis.

The selection of objects on the basis of their soft X-ray flux ensured that spectra with adequate statistics were obtained for the majority of the quasars observed by *Ginga*. However, such selection may significantly bias our sample: it has been argued (e.g., Elvis et al. 1986) that soft X-ray–selected quasar samples

TABLE 1

Ginga OBSERVATIONS OF HIGH-LUMINOSITY AGNs

Source Name	Common Name	z	N_H[a]	Start Time (UT)	Stop Time (UT)	Exposure[b] (s)
0637−752..........	PKS	0.66	5.0	1988 Jul 4 18:15	1988 Jul 5 16:27	12000
0804+761..........	PG	0.1	2.8	1989 Oct 31 03:35	1989 Oct 31 20:40	19000
0837−120..........	PKS	0.198	5.8	1989 Mar 27 10:59	1989 Mar 28 07:18	12000
1211+143..........	PG	0.09	2.7	1988 May 6 02:08	1988 May 6 18:08	9000
1217+023..........	PKS	0.24	1.9	1988 Jun 21 03:07	1988 Jun 21 23:42	19000
1219+755..........	Mrk 205	0.07	3.4	1988 Jan 16 03:30	1988 Jan 17 15:30	11000
1226+023..........	3C 273	0.158	1.8	1987 Jul 8 22:24	1987 Jul 11 00:01	17000
				1987 Dec 27 12:28	1987 Dec 30 04:52	28000
				1988 May 25 15:52	1988 May 26 12:30	14000
				1988 Jun 4 10:17	1988 Jun 5 16:16	12000
				1988 Dec 27 08:21	1988 Dec 28 03:11	13000
1307+085..........	PG	0.155	2.1	1989 Jun 6 04:14	1989 Jun 7 14:10	11000
1352+183..........	PG, E	0.152	2.0	1987 Jun 8 12:58	1987 Jun 19 11:01	15000
1407+265..........	PG	0.944	1.5	1987 Jun 19 11:02	1987 Jun 20 23:00	21000
1416−129..........	PG	0.129	6.8	1988 Feb 2 19:13	1988 Feb 3 22:38	19000
1821+643..........	E	0.297	3.5	1987 May 12 16:25	1987 May 14 23:55	12000
				1988 Oct 27 08:14	1988 Oct 27 18:23	11000
2130+099..........	PG, II Zw 136	0.061	4.6	1989 Nov 7 18:42	1989 Nov 8 17:59	14000
2135+147..........	PKS, PHL 1657	0.20	4.5	1988 May 10 22:52	1988 May 11 19:34	15000
2201+315..........	4C 31.63	0.297	9.2	1989 Nov 4 03:07	1989 Nov 5 13:18	23000

[a] Galactic column expressed in units of 10^{20} cm^{-2}.
[b] Approximate exposure (after data selection criteria applied).

are biased against flat spectra, and objects with significant intrinsic absorption will obviously not be favored. Moreover, radio-loud quasars are brighter in the X-ray region than radio-quiet quasars (Zamorani et al. 1981) and will be overrepresented in an X-ray–selected sample compared with an optically selected one.

The background was estimated using variations of the two methods described by Hayashida et al. (1989); both are based on modeling the various components of the background in terms of geomagnetic and other parameters. The "local" method (method I in Hayashida et al.) uses off-source observations taken within 2 days of the on-source observation to estimate the background, while the "universal" method (similar to method II in Hayashida et al.) uses all the off-source observations taken within a 4 month period to create a background model valid for any time during that period. The relative merits of the two techniques have been discussed in Hayashida et al. and in Turner et al. (1990). The limiting 90% error in the estimation of the internal background for both methods is good (<0.03 counts s^{-1} keV^{-1} in the 2–10 keV band), although the accuracy of the "local" method may be constrained by the statistics of the off-source observation. Fluctuations in the CXB, ~ 0.8 counts s^{-1} rms over the full energy range (Hayashida et al. 1989; Warwick & Stewart 1989), cause significant uncertainties for the weaker sources in our sample. The "local" background subtraction method estimates the CXB in an on-source observation from a single off-source observation, which results in an uncertainty of $\sqrt{2} \times 0.8$ counts s^{-1}.

The first observation of E1821+643 has not been analyzed using the "universal" background subtraction method (see Table 3). This is because a gradual rise in background observed during the first 6 months of operation (Hayashida et al. 1989) makes the current application of the universal method unreliable for observations during this period.

The background-subtracted pulse-height spectra were fitted with trial incident spectra using a standard χ^2 minimization technique. The errors quoted from the spectral fitting are, unless otherwise stated, 1 σ multiparameter errors, but note that they do not include uncertainties due to CXB fluctuations. In cases where these uncertainties are important, they are assessed separately, by methods described in the text. Within the limitations discussed above, results derived from the two background subtraction techniques are similar, and, unless explicitly stated, only results from "universal" subtractions are quoted.

All luminosities are calculated assuming $q_0 = 0$ and a Hubble constant of $H_0 = 50$ km s^{-1} Mpc^{-1}.

3. RESULTS

Fits were performed using a power law with both Galactic and intrinsic absorption, with an emission line at 6.4 keV (in the source rest frame). The Galactic absorption was fixed at the Stark et al. (1984) values listed in Table 1 (see also Elvis, Lockwood, & Wilkes 1989). The incident 2–10 keV flux, spectral (energy) index, intrinsic N_H, and reduced χ^2 derived from these fits are given in Tables 2 and 3 (using "local" and "universal" background subtractions, respectively). Tables 2 and 3 also include, for comparison purposes, the reduced χ^2 obtained from a power-law and absorption model *without* an emission line. For all observations, a single power law with intrinsic and Galactic absorption gave a value of the intrinsic N_H compatible with zero when the Galactic N_H was fixed at the Stark et al. (1984) value. Figure 1 shows the incident photon spectra for all the quasars.

We note that while a number of the observations show significant deviations from a simple power-law model, a power-law plus emission-line model is an adequate *empirical* description in the majority of cases. It is thus still useful to use the best-fit spectral index to characterize the continuum spectrum of a quasar over our energy range: § 3.2 gives the results from an analysis of the spectral indices of our quasar sample, while § 3.4 describes the results from attempts to model the deviations from the power law.

TABLE 2

FITS WITH POWER-LAW MODEL, WITH AND WITHOUT A 6.4 keV EMISSION LINE TO *Ginga* SPECTRA[a] AFTER "LOCAL" BACKGROUND SUBTRACTION

Name	α[a]	Continuum Flux[b,c]	N_H[d]	Line Flux[e]	χ^2/ν[f]	χ^2/ν[g]	F[h]
PKS 0637−752	$0.76^{+0.21}_{-0.11}$	0.86	$5.7^{+34}_{-5.7}$	$0.22^{+0.31}_{-0.22}$	32/25	34/26	1.5
PG 0804+761	$1.00^{+0.27}_{-0.14}$	0.60	$0.7^{+11}_{-9.7}$	$0.18^{+0.19}_{-0.18}$	23/25	27/26	3.8
PKS 0837−120[i]	...	...	...	...	...	...	...
PG 1211+143	$1.17^{+0.22}_{-0.15}$	0.61	$0.0^{+7.1}_{-0.0}$	$0.11^{+0.24}_{-0.11}$	32/25	33/26	0.8
PKS 1217+023	$0.74^{+0.38}_{-0.18}$	0.36	$0.1^{+21}_{-0.1}$	$0.03^{+0.20}_{-0.03}$	21/25	21/26	0.0
Mrk 205	$0.95^{+0.13}_{-0.11}$	1.01	$0.0^{+3.4}_{-0.0}$	$0.17^{+0.29}_{-0.17}$	43/25	61/26	7.6
3C 273	$0.52^{+0.04}_{-0.02}$	5.55	$1.4^{+1.7}_{-1.4}$	$0.46^{+0.24}_{-0.25}$	24/25	39/26	10
	$0.53^{+0.02}_{-0.01}$	12.4	$0.8^{+0.9}_{-0.8}$	$0.17^{+0.28}_{-0.17}$	29/25	31/26	1.7
	$0.46^{+0.01}_{-0.01}$	10.7	$0.0^{+0.5}_{-0.0}$	$0.26^{+0.36}_{-0.26}$	38/25	40/26	1.3
	$0.47^{+0.02}_{-0.02}$	10.2	$0.2^{+1.3}_{-0.2}$	$0.06^{+0.32}_{-0.06}$	21/25	21/26	0.0
	$0.44^{+0.03}_{-0.02}$	7.86	$1.1^{+1.9}_{-1.1}$	$0.34^{+0.34}_{-0.34}$	14/25	18/26	5.8
PG 1307+085	$1.26^{+0.37}_{-0.28}$	0.35	$0.0^{+12}_{-0.0}$	$0.00^{+0.25}_{-0.00}$	32/25	32/26	0.0
PG 1352+183[i]	...	...	...	...	...	...	...
PG 1407+265	...	0.15	...	...	22/25	22/26	0.0
PG 1416−129	$0.08^{+0.14}_{-0.12}$	0.74	$0.0^{+8.2}_{-0.0}$	$0.00^{+0.10}_{-0.00}$	47/25	47/26	0.0
E 1821+643	$1.04^{+0.11}_{-0.10}$	1.87	$7.8^{+8.6}_{-7.8}$	$0.40^{+0.34}_{-0.34}$	37/25	43/26	3.6
	$0.88^{+0.05}_{-0.04}$	1.73	$0.0^{+1.6}_{-0.0}$	$0.47^{+0.20}_{-0.20}$	26/25	51/26	12.7
II Zw 136	$1.39^{+0.22}_{-0.20}$	0.50	$0.0^{+3.0}_{-0.0}$	$0.20^{+0.23}_{-0.20}$	27/25	30/26	2.6
PHL 1657	$0.88^{+0.08}_{-0.07}$	1.24	$0.0^{+1.6}_{-0.0}$	$0.06^{+0.24}_{-0.06}$	43/25	43/26	0.0
4C 31.63	$0.73^{+0.34}_{-0.26}$	0.37	13^{+32}_{-13}	$0.12^{+0.19}_{-0.12}$	23/25	24/26	1.1

[a] Over the 1.7–17.36 keV range.
[b] Over the 2–10 keV range.
[c] Flux expressed in units of 10^{-11} ergs cm^{-2} s^{-1}.
[d] Measured column expressed in units of 10^{21} cm^{-2}.
[e] Flux expressed in units of 10^{-4} photons cm^{-2} s^{-1}.
[f] χ^2/ν for power law plus 6.4 keV emission line with cold absorber.
[g] χ^2/ν for power law with cold absorber.
[h] F-statistic, $\Delta\chi^2/\chi^2_\nu$, used to measure the significance of the reduction in χ^2 by the addition of the 6.4 keV iron line. $F > 3$ corresponds to greater than 90% significance.
[i] Local background not available.

3.1. *Effect of CXB Fluctuations*

In this section we quantify the effect of the CXB fluctuations on measurements of the spectral index α. We assume that these uncertainties follow a Gaussian distribution and therefore can be described by a single number σ_f. There are three approaches which can be used to estimate or place limits on σ_f.

First, the second column of Table 3 contains an estimate of the uncertainties due to CXB fluctuations on individual sources (shown as additional errors on the spectral indices). These numbers have been derived by adding and subtracting the rms *fluctuation* in the CXB to each observation. This method is used throughout this paper to estimate the effect of CXB fluctuations on individual sources, but should be noted that it only provides a relatively crude estimate because it assumes that the spectrum of the CXB fluctuations is constant, and also that the distribution of the CXB fluctuations is Gaussian. The mean of the uncertainties in Table 3 (0.07) gives an estimate of σ_f. The remaining methods enable upper and lower limits to be set to σ_f.

The second method exploits the differences between values of α, for individual sources, derived from "local" and "universal" background-subtracted spectra. These are discussed fully in § 2 and arise from the statistical limitations inherent in the "local" method as well as the effect of CXB fluctuations. The standard deviation, σ_d, of the distribution of spectral index differences ($\alpha_l - \alpha_u$) is therefore expected to be greater than σ_f. The 12 quasars which have both universal and local subtractions (see Tables 2 and 3), give the value of $\sigma_d = 0.13$, implying an *upper* limit $\sigma_f < 0.13$.

The third method exploits the differences between our observed distributions of α derived from "local" and "universal" background-subtracted spectra, and utilizes a technique described by Worrall & Wilkes (1990) to extract the residual width of the distribution of α, after allowing for measurement errors. The residual width in this case includes the effect of CXB fluctuations, and so the standard distribution obtained does not in this case correspond to the true intrinsic distribution, σ_i, but rather to σ_{i+f}. First the likelihood distribution for α was computed for each source, with the normalization and intrinsic absorption as free parameters. Then a maximum-likelihood analysis was used to find the mean power law, $\bar{\alpha}$, and the standard deviation, σ_{i+f}, of the "intrinsic" distribution (assuming that the "intrinsic" distribution, but *not* necessarily the observed distribution, is Gaussian). This method was applied to the universal background-subtracted data, to give $\bar{\alpha}_u$ and $\sigma_{u:i+f}$, and to the local background-subtracted data, to give $\bar{\alpha}_l$ and $\sigma_{l:i+f}$. Assuming Gaussian distributions, we expect $(\sigma_{l:i+f})^2 \sim (\sigma_{u:i+f})^2 + (\sigma_f)^2$, owing to the effect of CXB fluctuations on the single off-source observation used to assess the background in the "local" case. The sample of 12 quasars, which have both universal and local subtractions, gives the values $\bar{\alpha}_u = 0.81 \pm 0.21$, $\sigma_{u:i+f} = 0.31^{+0.20}_{-0.11}$,

TABLE 3

FITS WITH POWER LAW PLUS 6.4 keV EMISSION LINE MODEL TO *Ginga* SPECTRA AFTER "UNIVERSAL" BACKGROUND SUBTRACTION

		CONTINUUM[b]				LINE				
NAME	α[a]	Flux	Luminosity	N_H[c]	N_H[d]	Flux[e]	EW[j]	χ^2/ν[f]	χ^2/ν[g]	F[h]
PKS 0637−752	$0.83^{+0.15-0.02}_{-0.08+0.04}$	0.93	28.2	$0.0^{+19}_{-0.0}$	<79	$0.31^{+0.25}_{-0.26}$	200 ± 165	22/25	28/26	5.6
PG 0804+761	$1.08^{+0.16-0.07}_{-0.11+0.15}$	0.58	0.27	$0.0^{+5.4}_{-0.00}$	<59	$0.15^{+0.16}_{-0.15}$	<530	21/25	24/26	3.2
PKS 0837−120	$0.89^{+0.28-0.11}_{-0.17+0.23}$	0.56	1.12	$8.3^{+16}_{-8.3}$	<230	$0.00^{+0.19}_{-0.00}$	<300	16/25	16/26	0.0
PG 1211+143	$1.11^{+0.17+0.17}_{-0.13-0.11}$	0.77	0.29	$0.0^{+4.8}_{-0.0}$	<48	$0.11^{+0.23}_{-0.11}$	<450	19/25	20/26	1.3
PKS 1217+023	$0.49^{+0.19+0.05}_{-0.11+0.04}$	0.56	1.56	$0.0^{+13}_{-0.0}$	<130	$0.00^{+0.06}_{-0.00}$	<290	34/25	34/26	0.0
Mrk 205	$0.91^{+0.09-0.03}_{-0.08+0.03}$	0.90	0.20	$0.0^{+1.0}_{-0.0}$	<12	$0.27^{+0.18}_{-0.18}$	300 ± 200	41/25	51/26	4.9
3C 273	$0.53^{+0.02-0.01}_{-0.01+0.01}$	5.97	6.95	$1.9^{+1.4}_{-1.5}$	<27	$0.36^{+0.22}_{-0.22}$	54 ± 27	18/25	30/26	10
	$0.53^{+0.01-0.01}_{-0.01+0.01}$	13.5	15.7	$0.0^{+0.8}_{-0.0}$	<9	$0.22^{+0.28}_{-0.22}$	<31	20/25	22/26	2.3
	$0.47^{+0.01-0.01}_{-0.02+0.01}$	10.0	11.6	$0.0^{+0.9}_{-0.0}$	<9	$0.30^{+0.33}_{-0.30}$	<57	26/25	30/26	2.6
	$0.46^{+0.02-0.01}_{-0.01+0.01}$	10.7	12.5	$0.1^{+1.5}_{-0.1}$	<13	$0.32^{+0.34}_{-0.32}$	<56	17/25	20/26	2.6
	$0.44^{+0.02-0.01}_{-0.01+0.01}$	10.0	11.6	$0.0^{+1.4}_{-0.0}$	<18	$0.22^{+0.34}_{-0.22}$	<50	45/25	47/26	1.1
PG 1307+085	$0.86^{+0.15-0.03}_{-0.08+0.05}$	0.64	0.75	$0.0^{+2.8}_{-0.0}$	<25	$0.00^{+0.18}_{-0.00}$	<280	35/25	35/26	0.0
PG 1352+183	...	0.16	0.17	...	...	...	...	29/25	29/26	0.0
PG 1407+265	...	0.15	8.28	...	...	...	...	22/25	22/25	0.0
PG 1416−129	$0.10^{+0.11+0.11}_{-0.10-0.19}$	0.66	0.48	$0.0^{+3.2}_{-0.0}$	<33	$0.00^{+0.15}_{-0.00}$	<250	41/25	41/26	0.0
E1821+643[i]	...	...	...	...	...	...	...	...	...	...
	$0.93^{+0.10-0.03}_{-0.07+0.04}$	1.87	9.16	$2.8^{+6.3}_{-2.8}$	...	$0.54^{+0.21}_{-0.26}$	235 ± 120	18/25	36/26	13
II Zw 136	$1.29^{+0.19-0.14}_{-0.16+0.26}$	0.48	0.08	$0.0^{+1.5}_{-0.0}$	<15	$0.06^{+0.20}_{-0.06}$	<600	37/25	37/26	0.0
PHL 1657	$0.81^{+0.06-0.01}_{-0.06+0.01}$	1.18	2.26	$0.0^{+1.0}_{-0.0}$	<12	$0.00^{+0.08}_{-0.00}$	<140	62/25	63/25	0.4
4C 31.63	$0.69^{+0.15+0.01}_{-0.15-0.04}$	0.35	1.61	$0.0^{+8.5}_{-0.0}$	<86	$0.02^{+0.17}_{-0.02}$	<450	18/25	18/26	0.0

[a] Over the 1.7–17.36 keV range.
[b] Over the 2–10 keV range. Flux in units of 10^{-11} ergs cm^{-2} s^{-1}. Luminosity in units of 10^{45} ergs s^{-1}.
[c] Measured absorbing column, expressed as equivalent hydrogen in units of 10^{21} cm^{-2}.
[d] Measured cold iron edge, expressed as equivalent hydrogen in units of 10^{21} cm^{-2}.
[e] Flux in units of 10^{-4} photons cm^{-2} s^{-1}.
[f] χ^2/ν for power law plus 6.4 keV emission line with cold absorber.
[g] χ^2/ν for power law with cold absorber.
[h] F statistic, $\Delta\chi^2/\chi^2_\nu$, used to measure the significance of the reduction in χ^2 by the addition of the 6.4 keV iron line. $F > 3$ corresponds to greater than 90% significance.
[i] Universal background subtraction not applicable (see § 2).
[j] Equivalent width in source rest frame expressed in eV.

$\bar{\alpha}_l = 0.89 \pm 0.19$, $\sigma_{l:i+f} = 0.29^{+0.19}_{-0.09}$. In fact, $\sigma_{u:i+f} < \sigma_{l:i+f}$, which shows that for this case $\sigma_f \sim 0$. We therefore adopt this as a lower limit to σ_f.

We conclude that we can estimate $\sigma_f = 0.07 \pm 0.07$.

3.2. *Power-Law Spectral Indices*

The majority of the 2–10 keV spectral indices presented in Tables 2 and 3 are close, but not identical, to the "canonical" value determined for the lower luminosity objects by, e.g., Turner & Pounds (1989). The mean spectral index for all the quasars in Table 3 is $\bar{\alpha} \sim 0.81$, with an observed standard deviation of $\sigma_o = 0.29$. A simple χ^2 test can be used to test whether the distribution of α observed by *Ginga* is consistent with an intrinsic width, σ_i, of zero, with the observed width, σ_o, arising solely from measurement errors due to statistical limitations and background fluctuations. The value of χ^2/ν obtained is 137/13, which is clearly *inconsistent* with $\sigma_i \sim 0$. Note, however, that this is dominated by the two quasars, 3C 273 and PG 1416−129, which have spectra which are significantly flatter than the canonical value: $\alpha \sim 0.5$ for 3C 273 and $\alpha \sim 0.1$ for PG 1416−129. Removing these two flat-spectrum quasars from the sample gives $\bar{\alpha} = 0.90$, $\sigma_o = 0.20$, $\chi^2/\nu = 16/11$.

In order to quantify the intrinsic width of the distributions, we again make use of the method described by Worrall & Wilkes (1990), used in § 3.1 to investigate the effect of CXB fluctuations. A likelihood distribution for α was computed for each of the 13 quasars in our sample, and a maximum-likelihood analysis was used to find the mean power-law index, $\bar{\alpha} = 0.81 \pm 0.19$, and the standard deviation of the "intrinsic" distribution, $\sigma_{i+f} = 0.29^{+0.20}_{-0.09}$. As noted above, this procedure does not take account of errors due to CXB fluctuations, so the deviation obtained corresponds to σ_{i+f} rather than the true intrinsic deviation, σ_i. However, using the value $\sigma_f = 0.07 \pm 0.07$ (derived in § 3.1 from the difference between "local" and "universal" background subtractions), and assuming Gaussian distributions (so that $\sigma_i^2 \sim \sigma_{i+f}^2 - \sigma_f^2$), we can obtain a value $\sigma_i = 0.28^{+0.21}_{-0.10}$ for the true intrinsic distribution. If we apply a similar analysis, excluding the two flat-spectrum quasars 3C 273 and PG 1416−129, we obtain $\bar{\alpha} = 0.92 \pm 0.19$, $\sigma_{i+f} = 0.20^{+0.14}_{-0.09}$, and $\sigma_i = 0.19^{+0.15}_{-0.10}$, i.e., there *is* a residual dispersion.

We can compare these numbers with those of Worrall (1989), who has used a maximum-likelihood analysis to separate the intrinsic dispersion of spectral index from the measurement errors for a number of X-ray–observed samples of AGNs. The results of Worrall, together with the new *Ginga* results, are reproduced here in Table 4. We see that the mean spectral index and intrinsic width of the entire *Ginga* sample are broadly compatible with results from the previous spectral

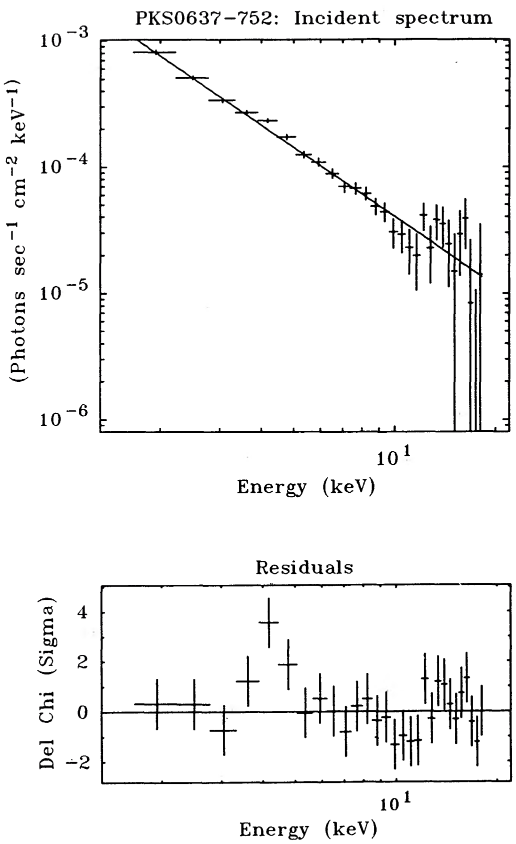

FIG. 1*a*

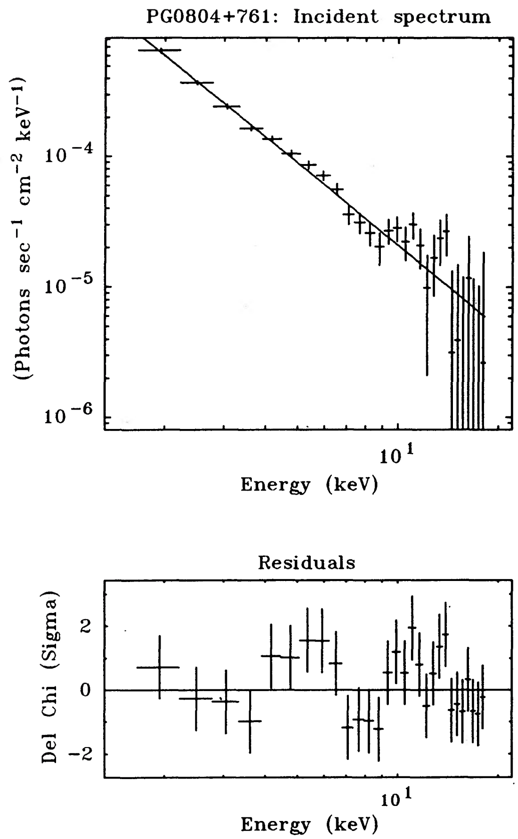

FIG. 1*b*

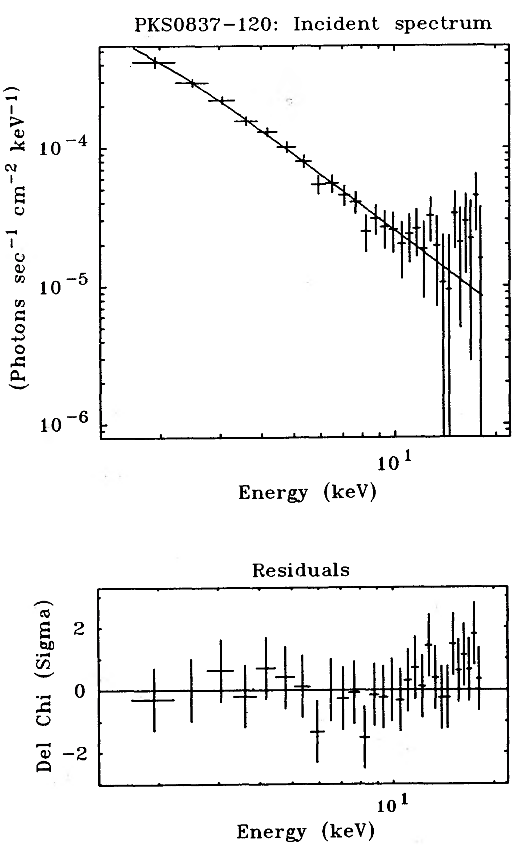

FIG. 1*c*

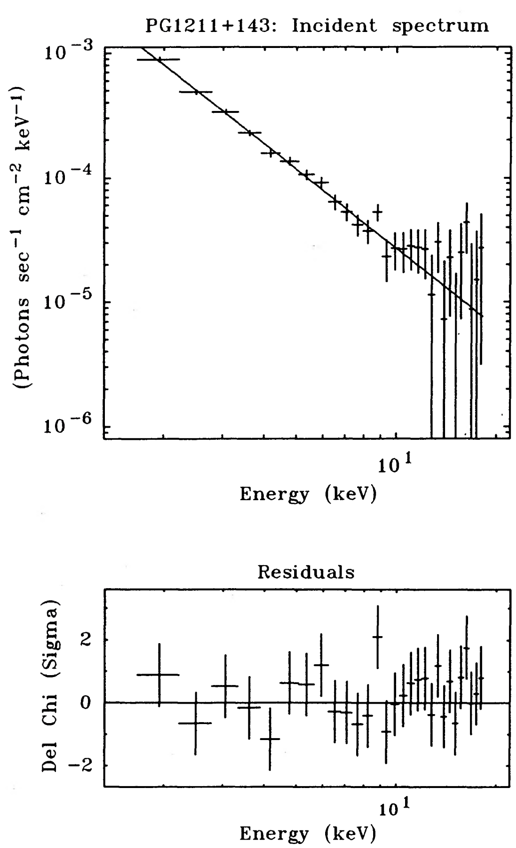

FIG. 1*d*

FIG. 1.—*Ginga* spectra, and residuals to a power-law fit, shown over the range ~1.5–18.0 keV

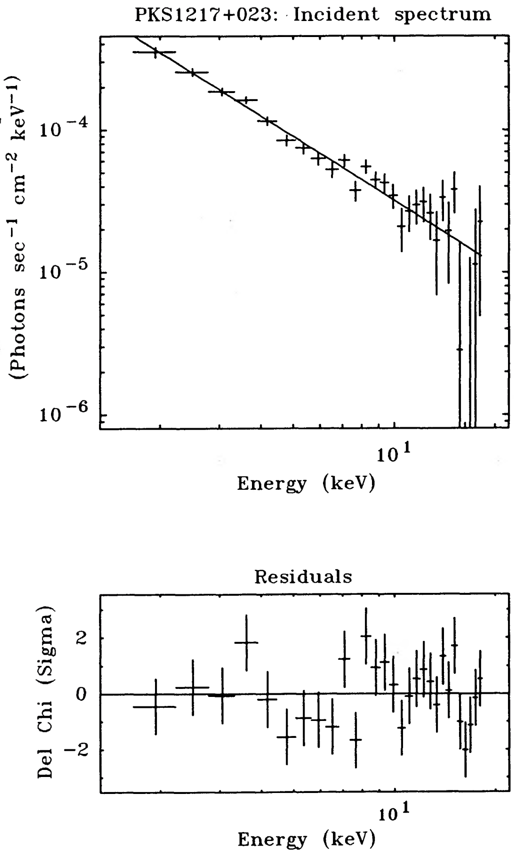

FIG. 1*e*

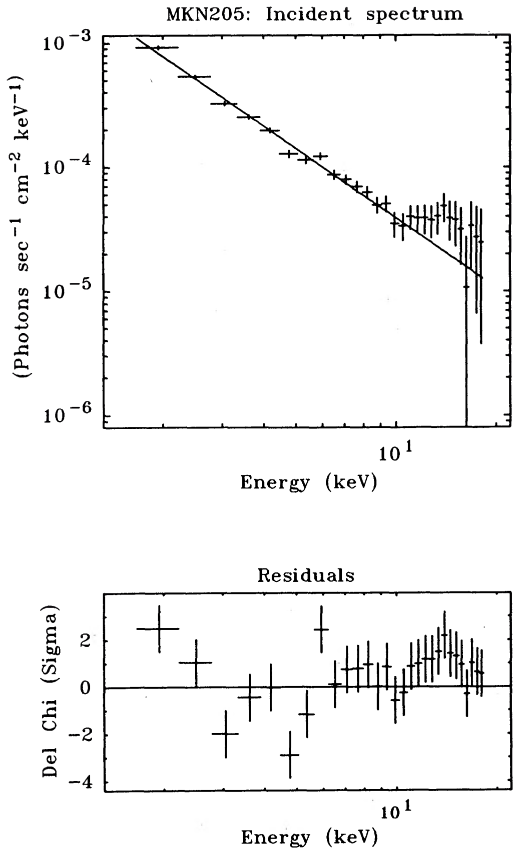

FIG. 1*f*

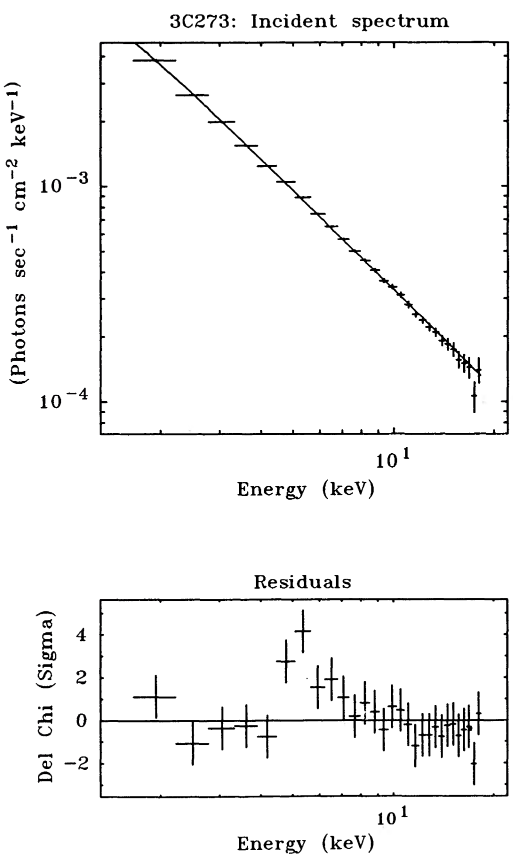

FIG. 1*g*

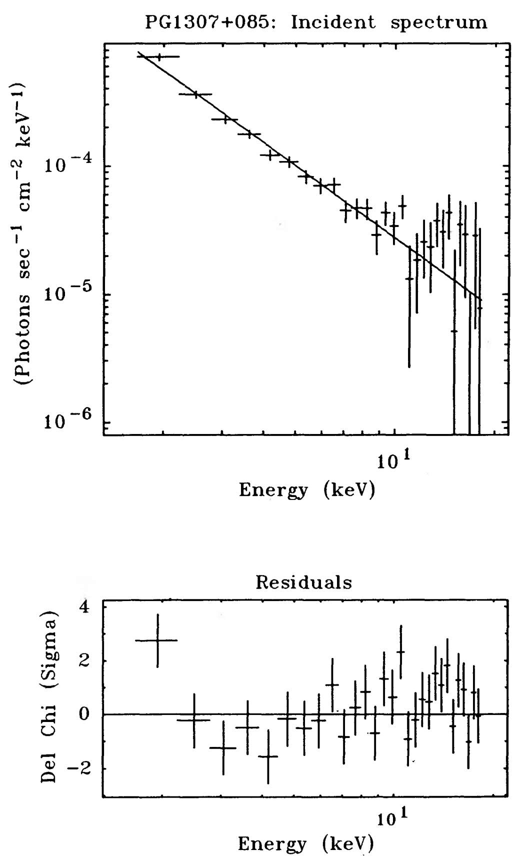

FIG. 1*h*

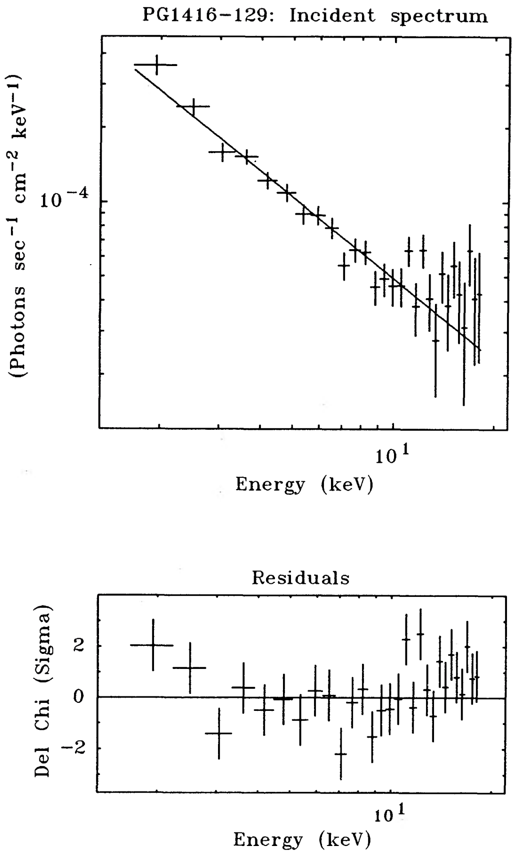

FIG. 1*i*

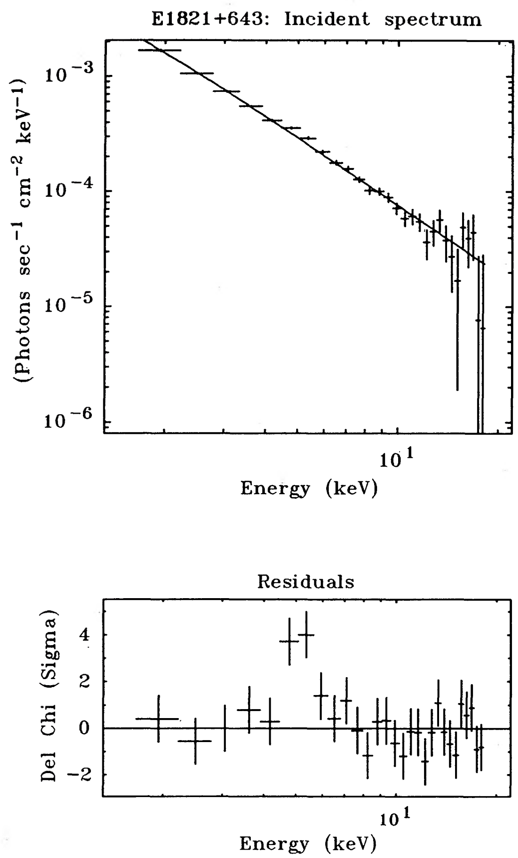

FIG. 1*j*

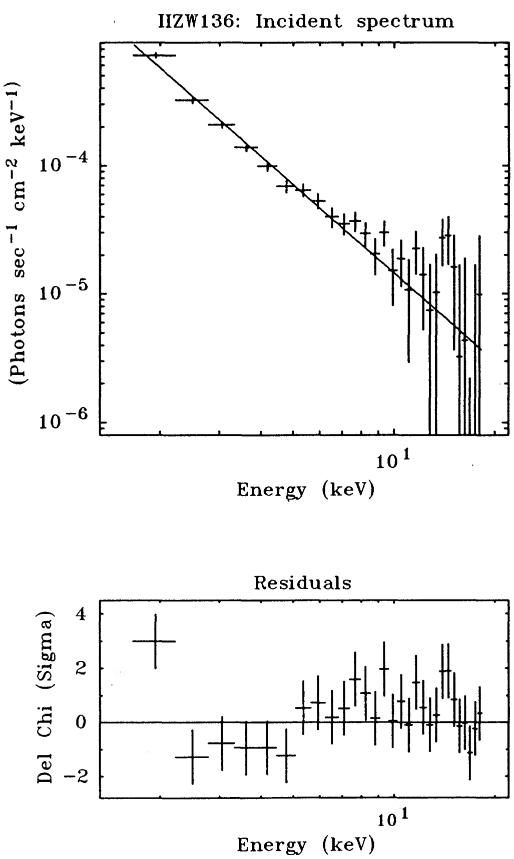

FIG. 1*k*

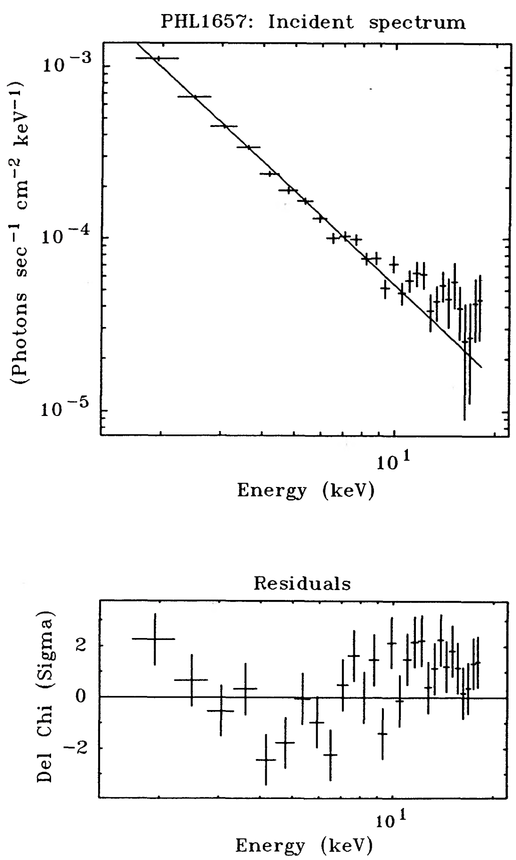

FIG. 1*l*

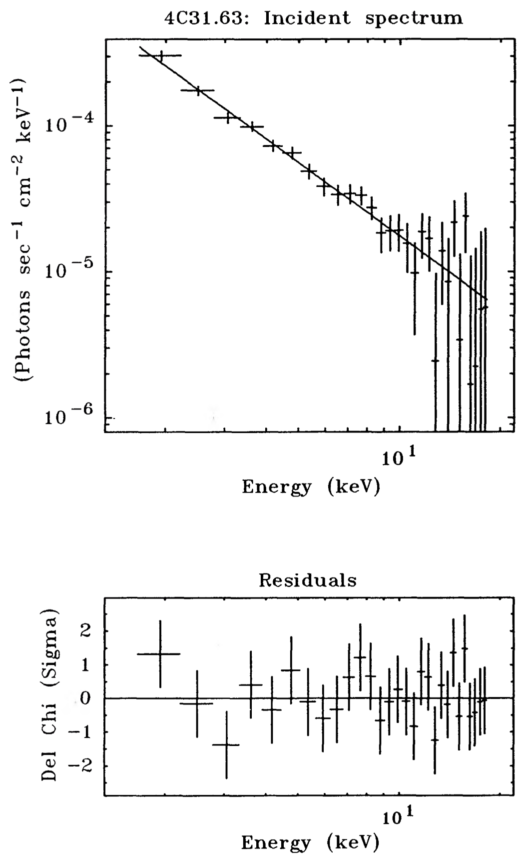

FIG. 1m

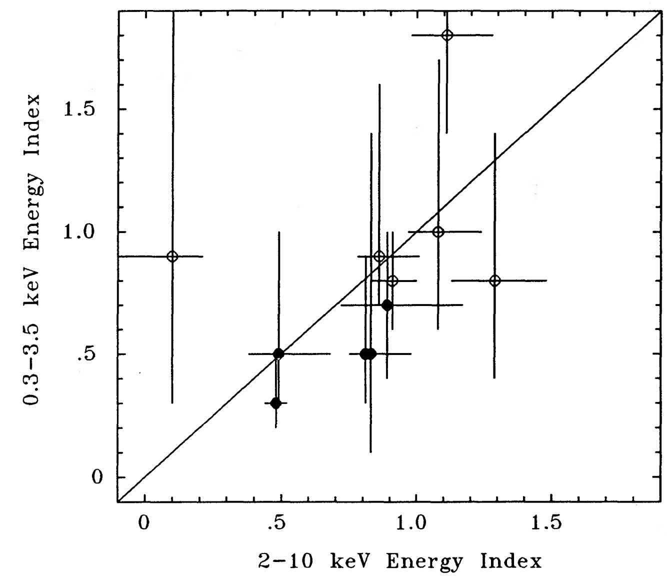

FIG. 2.—Spectral index measured by *Einstein* shown against that measured by *Ginga*. *Einstein* errors are 90% confidence limits. Radio-loud quasars are shown as filled circles and radio-quiet quasars as open circles.

surveys, although we note that the three surveys consisting mainly of Seyfert galaxies have narrower distributions than the two surveys confined to quasars.

In view of the link between the X-ray and radio properties of quasars (see § 1), we have repeated the above dispersion analysis with radio-loud and radio-quiet quasars separated (see § 2); the results of this analysis are included in Table 4.

Worrall (1989) divided the Wilkes & Elvis (1987) sample into radio-loud and radio-quiet subsamples, and found that the radio-loud sample had a dispersion consistent with zero, while the radio-quiet sample had a dispersion 0.4 ± 0.2. Our results are broadly compatible with this, and although the size of the dispersion depends strongly on the peculiar result from PG 1416−129, the radio-quiet quasars still show significant dispersion after the removal of this quasar from the sample (see Table 4).

Figure 2 shows the spectral indices observed by *Einstein* plotted against those observed by *Ginga*. The *Einstein* values are from Wilkes & Elvis (1987), except for PG 0804+761, $\alpha = 1.0^{+0.7}_{-0.4}$, and PKS 0837−120, $\alpha = 0.7^{+0.3}_{-0.3}$ (B. J. Wilkes 1990, private communication). A linear regression analysis yields $\alpha(Ginga) = 1.06(\pm 0.39) \times \alpha(Einstein) - 0.15(\pm 0.29)$,

TABLE 4

MEAN AND INTRINSIC DISPERSION OF X-RAY SPECTRAL INDICES, AS CALCULATED BY WORRALL 1989, COMPARED WITH *Ginga* RESULT

Sample	90% Confidence Range of $\bar{\alpha}$	Best Fit and 90% Confidence Range of σ_i	Energy Range (keV)	Reference
Ginga QSOs	0.62–1.00	$0.28^{+0.21}_{-0.10}$	2–10	This paper
Ginga QSOs[a]	0.73–1.11	$0.19^{+0.15}_{-0.10}$	2–10	This paper
Ginga RQ QSOs	0.57–1.25	$0.34^{+0.37}_{-0.12}$	2–10	This paper
Ginga RQ QSOs[b]	0.88–1.19	$0.13^{+0.17}_{-0.06}$	2–10	This paper
Ginga RL QSOs	0.56–0.86	$0.14^{+0.16}_{-0.07}$	2–10	This paper
Ginga RL QSOs[c]	0.63–0.87	$0.10^{+0.11}_{-0.09}$	2–10	This paper
HEAO 1 A2 Seyferts	0.62–0.76	$0.15^{+0.06}_{-0.05}$	2–50	Mushotzky 1984
SSS Seyferts/QSOs	0.55–0.82	$0.27^{+0.13}_{-0.09}$	0.75–4.5	Petre et al. 1984
IPC QSOs	0.57–0.90	$0.30^{+0.14}_{-0.10}$	0.1–3.5	Wilkes & Elvis 1987
EXOSAT Seyferts	0.67–0.79	$0.15^{+0.06}_{-0.04}$	0.1–10	Turner & Pounds 1989
IPC Seyferts	0.75–0.97	$0.19^{+0.12}_{-0.09}$	0.1–3.5	Kruper et al. 1990

[a] Excluding 3C 273 and PG 1416−129.
[b] Radio-quiet quasars excluding PG 1416−129.
[c] Radio-loud quasars excluding 3C 273.

TABLE 5

RESULTS FROM RADIO AND OPTICAL OBSERVATIONS OF HIGH-LUMINOSITY AGNS

Name	B-Magnitude	f_B [a] (mJy)	Fe II EW (Å)	R_L [b]	f_R [c] (mJy)	References: Radio	References: Optical	References: Fe II
PKS 0637−752	16.08	1.64	...	3.52	5490	1	10	
PG 0804+761	15.15	3.87	...	−0.60	0.97	2	10	
PKS 0837−120	15.78	2.16	...	1.92	167	3	10	
PG 1211+143	14.63	6.25	38	−0.07	1.2	2	11	13
PKS 1217+023	16.55	1.07	<3	2.38	257	4	10	13
Mrk 205	15.64	2.47	20	−0.31	1.2	5	12	14
3C 273	13.07	26.30	10	3.06	30500	6	10	13
PG 1307+085	15.28	3.44	<3	−0.99	0.35	2	10	13
PG 1352+183	15.58	2.60	...	−0.01	0.25	2	10	
PG 1407+265	15.73	2.27	...	0.44	6.2	5	11	
PG 1416−129	15.40	3.08	<3	0.07	3.6	5	11	13
E1821+643	14.10	10.17	...	<0.17	<15	7	10	
II Zw 136	14.92	4.78	66	0.37	2.05	5	10	13
PHL 1657	15.63	4.79	<3	1.70	126	8	10	13
4C 31.63	15.56	2.49	...	2.90	2100	9	10	

[a] Calculated from m_B using $m_B(0) = 4440$ Jy; Johnson 1966.
[b] Radio-loudness as defined by Wilkes & Elvis 1987.
[c] Radio flux at 5 GHz.
REFERENCES.—(1) Savage 1976; (2) Kellermann et al. 1989; (3) Miley & Hartsuijker 1978; (4) Neff & Browne 1984; (5) Wilkes & Elvis 1987 and references therein; (6) Perley 1982; (7) Kolman et al. 1991; (8) Shimmins & Bolton 1972; (9) Zensus et al. 1984; (10) Hewitt & Burbidge 1987 and references therein; (11) Schmidt & Green 1983; (12) Véron-Cetty & Véron 1984; (13) Zheng & O'Brien 1990 and references therein; (14) Sulentic & Arp 1987.

showing that there is a significant correlation between the *Ginga* and *Einstein* spectral slopes. There are no significant differences in the measurements for the majority of quasars, the possible exceptions being PG 1416−129 (*Ginga:* $\alpha = 0.10 \pm 0.11$; *Einstein:* $\alpha = 0.9^{+1.3}_{-0.6}$) and PG 1211+143 (*Ginga:* $\alpha = 1.11^{+0.17}_{-0.12}$, *Einstein:* $\alpha = 1.8^{+0.5}_{-0.4}$). We note that PG 1211+143 has a particularly prominent soft excess, which may account for the discrepancy in this case. We have tested this by fitting *EXOSAT* ME 2–10 keV data (from the *EXOSAT* data base) with a power-law plus absorption model, which gives a spectral index of $\alpha = 1.08 \pm 0.19$ (compatible with the *Ginga* results), while fitting the combined LE/ME 0.3–10 keV data with the same model yields $\alpha = 1.75 \pm 0.05$ (compatible with the *Einstein* results).

3.3. *Correlation Analysis*

In this section we describe the search for correlations among the following parameters:

1. The 2–10 keV continuum flux measured by *Ginga* (Table 3).
2. The 2–10 keV X-ray luminosity (Table 3).
3. The X-ray spectral index, α_X, measured by *Ginga* (Table 3).
4. The radio-loudness parameter, R_L (Table 5). This is defined as the logarithm of the ratio of the 5 GHz radio flux (Table 5) and the *B*-band optical flux (Table 5), and is the same as that used by Wilkes & Elvis (1987) in their analysis of soft X-ray spectra of quasars measured with *Einstein.*
5. The redshift, *z* (Table 1).
6. The equivalent width of the optical Fe II emission lines (Table 5).
7. The *J*, *H*, *K*, and 25 μm (IR) band fluxes f_J, f_H, f_K, and f_{25} (Table 6).
8. The *J*, *H*, *K*, and 25 μm (IR) band luminosities, L_J, L_H, L_K, and L_{25} (derived from data in Table 6). The *J*, *H*, *K*, and 25 μm band luminosities are *K*-corrected using the *H*, *K*, *L*, and 60 μm data, respectively.
9. The spectral indices, α_{JH} and α_{HK}, of power laws joining the *J* to *H* and *H* to *K* (IR) bands (derived from the *K*-corrected luminosities).

Table 7 gives the results of a Spearman rank correlation analysis of the 2–10 keV X-ray luminosity, the 2–10 keV flux, and the 2–10 keV spectral index with each other, and with the other parameters. The numbers given are the two-sided significance levels of the deviation of Spearman's rank correlation r_S from zero, expressed as the probability that an observed correlation could occur by chance for uncorrelated data sets (see, e.g., Press et al. 1986). We note that if apparent correlations were due to problems with the background subtraction, we might expect strong correlations with the observed X-ray flux, f_X. However, Figure 3 shows no relationship between f_X and the X-ray spectral index, α_X, and Table 7 does not indicate any correlation between the X-ray *flux* and other parameters, except for the flux–flux relationships discussed below.

Table 7 shows a highly significant correlation (~99.999% significance) between the X-ray luminosity and redshift (see Fig. 4); this is expected because of the relatively narrow range of fluxes in our quasar sample. We further note a correlation (~99.9% significance) between luminosity and radio-loudness, previously noticed and discussed by, for example, Zamorani et al. (1981) and Kembhavi, Feigelson, & Singh (1986). These two dependencies result in a further apparent correlation observed between the radio-loudness and redshift; this correlation is not shown in Table 7 but has a significance of ~99%.

More interestingly, we also note possible correlations, although significant only at the 90% level, between α_X and R_L (see Fig. 5), α_X and luminosity (see Fig. 6), and α_X and *z* (see Fig. 7). However as discussed above, the radio-loudness, luminosity, and redshift are not independent in our sample, so we have carried out a partial Spearman rank correlation analysis

TABLE 6

INFRARED FLUXES OF *Ginga* QUASAR SAMPLE

Source	F_J (mJy)	F_H (mJy)	F_K (mJy)	$F_{25\,\mu m}$	References J, H, K	References 25 μm
PKS 0637−752	4.35 ± 0.08	4.88 ± 0.09	6.93 ± 0.13	...	1	
PG 0804+761	8.91 ± 0.62	12.88 ± 0.89	25.12 ± 1.74	209 ± 27	2	5
PKS 0837−120	1.74 ± 0.20	1.95 ± 0.22	3.31 ± 0.38	49 ± 16	3	6
PG 1211+143	10.50 ± 0.70	14.80 ± 1.00	26.30 ± 1.80	362 ± 51	2	6
PKS 1217+023	1.88 ± 0.04	2.56 ± 0.05	3.74 ± 0.10	...	1	
Mrk 205	7.41 ± 0.51	10.23 ± 0.71	13.18 ± 0.61	...	3	
3C 273	32.70 ± 2.30	41.80 ± 2.90	58.80 ± 4.10	941 ± 27		6
PG 1307+085	3.55 ± 0.25	4.37 ± 0.40	6.92 ± 0.48	<153	2	5
PG 1352+183	2.57 ± 0.30	3.09 ± 0.14	5.25 ± 0.24	<113	2	5
PG 1407+265	1.66 ± 0.19	1.74 ± 0.12	1.62 ± 0.15	<100	2	5
PG 1416−129	3.39 ± 0.23	3.47 ± 0.24	5.62 ± 0.39	<180	2	5
E1821+643	8.8	13.0	22.1	373 ± 18	4	6
II Zw 136	8.13 ± 0.56	13.80 ± 1.27	25.10 ± 1.80	380 ± 10	2	5
PHL 1657	3.31 ± 0.38	4.27 ± 0.29	7.24 ± 0.33	...	3	
4C 31.63	4.27 ± 0.49	6.17 ± 0.43	10.96 ± 0.76	111 ± 7	3	6

REFERENCES.—(1) Hyland & Allen 1982; (2) Neugebauer et al. 1987; (3) Neugebauer et al. 1979; (4) Kolman et al. 1991; (5) Sanders et al. 1989; (6) Neugebauer et al. 1986.

(e.g., Macklin 1982; Fabbiano, Gioia, & Trinchieri 1988) in an attempt to determine the fundamental correlation. Table 8 shows that it is impossible to determine which of the three parameters is fundamentally correlated with α_X: this is because, with the exception of E1821+643, there is no overlap between the ranges of luminosity and redshift covered by our radio-quiet and radio-loud quasars. Table 8 does not include 1E 1821+643, since it has not been detected at 5 GHz: if it is included using the upper limit to its radio flux, then the suggestion that L_X versus α_X is fundamental disappears. A relationship between radio-loudness and α_X has already been established for quasars in the soft X-ray band by Wilkes & Elvis (1987); therefore, we have investigated the specific possibility that the X-ray properties of quasars are divided into two populations depending on their radio-loudness. Applying the Kolmogorov–Smirnov (KS) test, we found that the probability that the distributions of the X-ray spectral index α_X for radio-loud and radio-quiet quasars are drawn from the same population is only 7%.

Table 7 also reveals significant correlations linking the X-ray and the IR parameters. The most significant (>99.99%) are between the X-ray luminosity (L_X) and the near-IR luminosities (L_J, L_H, and L_K), but there are also corresponding relationships between the X-ray and near-IR fluxes, albeit at lower (95%) significance. These correlations are illustrated in Figures 8*a* and 8*b*, which show the *J*-band flux and luminosity, L_J and f_J, plotted against the X-ray flux and luminosity, L_X and f_X, respectively. To investigate the relationship between L_X and L_J we need to allow for the contribution to the *J* band from starlight from the host galaxy, which will be of the order

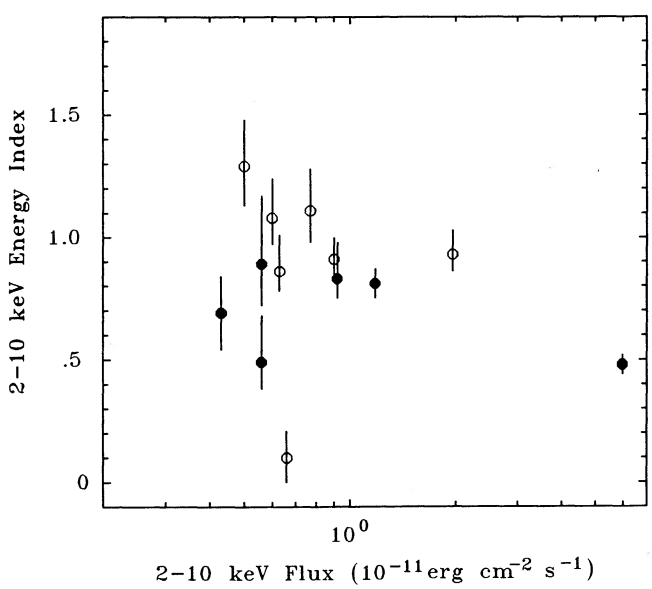

FIG. 3.—Variation of the spectral index measured by *Ginga* with detected flux (10^{-11} ergs cm^{-2} s^{-1}).

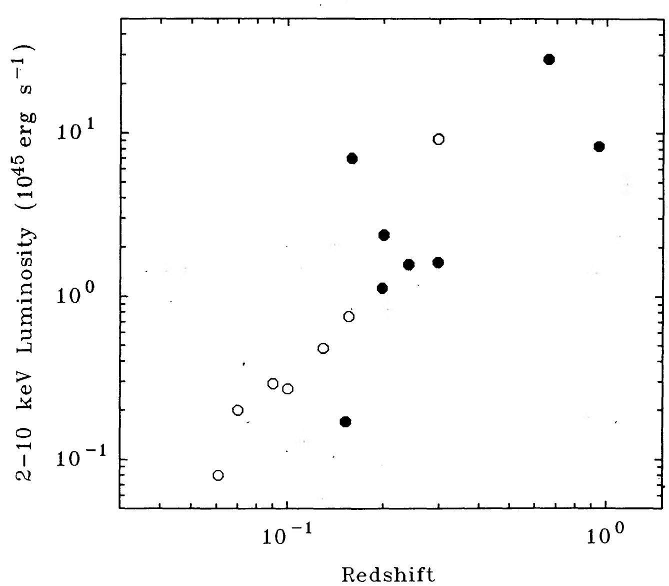

FIG. 4.—Variation of the 2–10 keV luminosity (ergs s^{-1}) measured by *Ginga* with redshift.

TABLE 7

SIGNIFICANCE OF SPEARMAN RANK CORRELATION ANALYSIS

Parameter	α_X	L_X	f_X	R_L	z	α_{JH}	α_{HK}
α_X	...	7.8×10^{-2}	0.62	9.5×10^{-2}	9.2×10^{-2}	6.1×10^{-2}	0.13
L_X	7.8×10^{-2}	...	0.17	1.4×10^{-3}	7.2×10^{-6}	0.54	0.39
f_X	0.62	0.17	...	0.42	0.90	0.72	0.63

Parameter	L_J	L_H	L_K	$L_{25\,\mu m}$	f_J	f_H	f_K	$f_{25\,\mu m}$
α_X	0.24	0.32	0.40	0.12	0.14	0.12	0.14	0.82
L_X	1.1×10^{-6}	2.4×10^{-6}	1.6×10^{-5}	4.5×10^{-4}	0.70	0.65	0.58	0.82
f_X	0.38	0.32	0.22	0.18	2.5×10^{-2}	4.0×10^{-2}	3.7×10^{-2}	0.18

of 10^{29} ergs s^{-1} Hz^{-1} for a galaxy of $10^{10}\ L_\odot$. Ignoring the contribution from starlight yields $L_X \propto L_J^{1.10\pm0.12}$, while assuming a starlight luminosity of 2×10^{29} ergs s^{-1} Hz^{-1} yields $L_X \propto L_J^{1.07\pm0.12}$.

In addition to the relationship between the near-IR and X-ray luminosities, Table 7 shows that there is a possible correlation between the near-IR spectral index α_{JH} and the X-ray spectral index α_X ($\sim$95% significance). The α_X versus α_{JH} data are shown in Figure 9 and can be fitted by $\alpha_X = -0.08 + 0.63\alpha_{JH}$. Inspection of Figure 9 shows that while the full data set has a large scatter about the correlation, the radio quiet quasars have a much smaller scatter. They can be fitted by $\alpha_X = -0.08 + 0.69\alpha_{JH}$; this relationship is influenced strongly by the data points corresponding to PG 1416−129 and II Zw 136. Figure 10 and Table 7 show that the evidence for corresponding correlations involving α_{HK} instead of α_{JH} is weaker.

Berriman (1990) has reported that the ratios of H- to J-band fluxes (colors) of PG quasars decline continuously with redshift, while the ratios of K- to H-band fluxes decline with redshift above values of $z \sim 0.3$. Berriman notes that this arises through redshifted optical emission moving into the IR pass-band. Many of our high-redshift objects have rather flat X-ray spectra (see above), and so this might lead to an apparent correlation between the near-IR flux ratios and α_X. We consider it unlikely, however, that this effect gives rise to the observed relationship between α_X and α_{JH}, first because we have used K-corrected luminosities (albeit based only on broad-band flux measurements) to calculate α_{JH}, and second because the spurious f_J/f_H versus α_X correlation would, in any case, be extremely weak for our sample. The results reported in Table 9 confirm this conclusion: for the *Ginga* sample α_{JH} is not significantly correlated with the redshift, or with any other parameter of interest.

The α_X/α_{JH} correlation is of low significance (95%), and there is no corroborative evidence from other surveys, unlike the α_X/R_L correlation. Consequently, we have sought data, from earlier instruments, with which to expand our sample. We have included data from *Einstein* imaging proportional counter (IPC) observations of five quasars (Wilkes et al. 1989) for which there are no corresponding *Ginga* observations: PG 0026+124, NAB 0205−024, PG 1426+015, 1501+106, and PG 1613+658. Infrared, B-band, and radio data for these quasars were taken from the references in Table 5. We have also included *EXOSAT* data from high-luminosity ($L_X < 10^{44}$

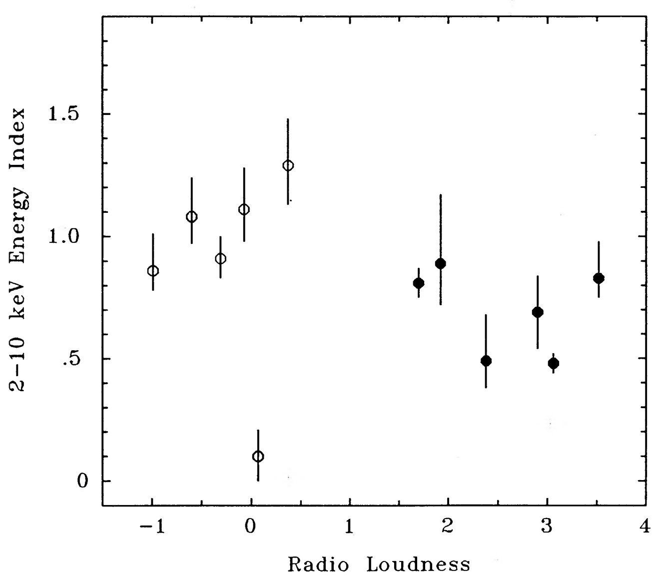

FIG. 5.—Variation of the spectral index measured by *Ginga* with R_L

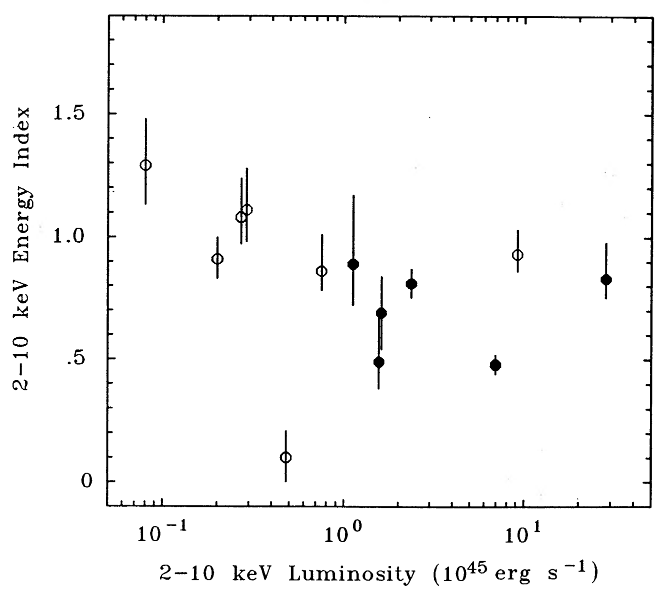

FIG. 6.—Variation of the spectral index measured by *Ginga* with luminosity (10^{45} ergs s^{-1}).

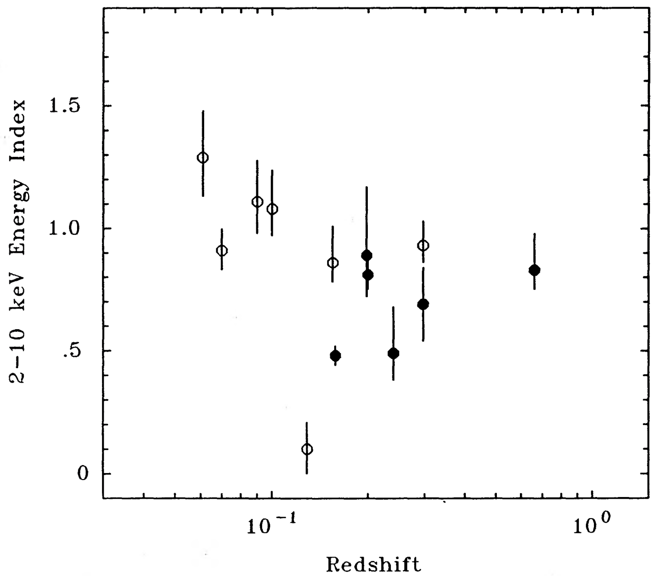

FIG. 7.—Variation of the spectral index measured by *Ginga* with redshift

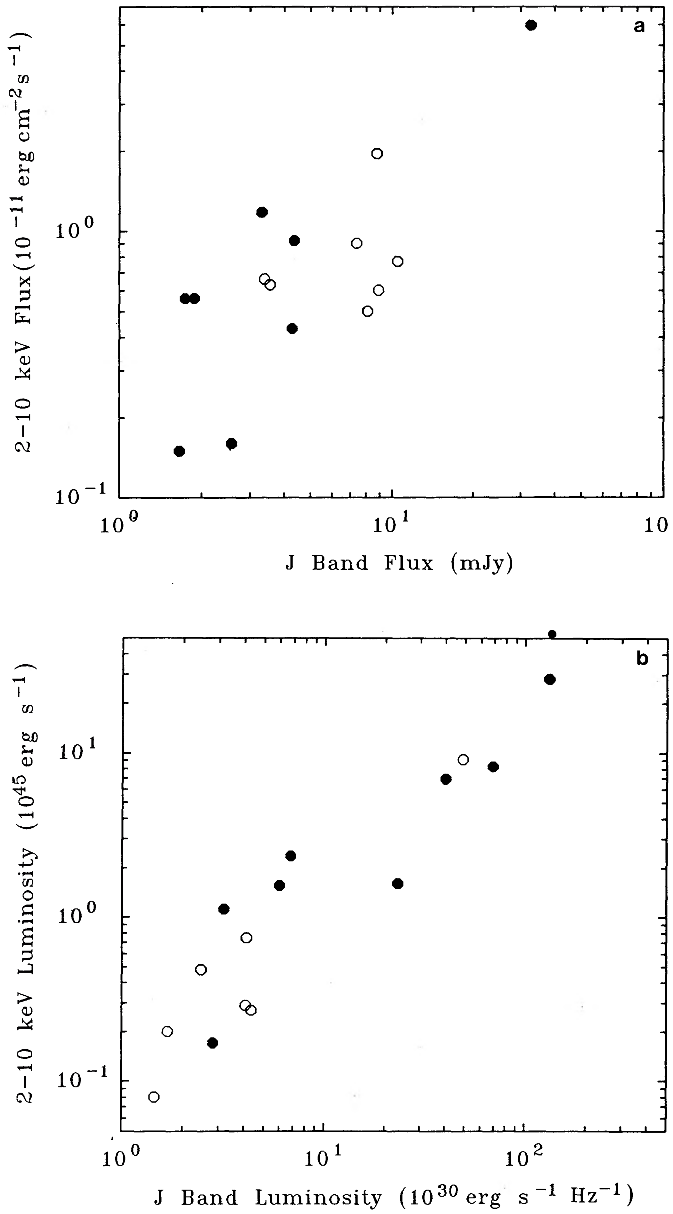

FIG. 8.—(*a*) Variation of the 2–10 keV flux (10^{-11} ergs cm^{-2} s^{-1}) measured by *Ginga* with the *J*-band flux (mJy). (*b*) Variation of the 2–10 keV luminosity (10^{45} ergs s^{-1}) measured by *Ginga* with the *J*-band luminosity (10^{30} ergs s^{-1} Hz^{-1}).

ergs s^{-1}) Seyfert I galaxies taken from Turner & Pounds (1989): IC 4329A, Mrk 509, Akn 120, and MR 2251. However, we are mindful that we may be including objects of a different nature: MR 2251, at least, is known to have a complex X-ray spectrum with significant absorption. Spectral slopes which were constrained to worse than $\sigma_\alpha \sim 0.3$ were not used. IR data were taken from Ward et al. (1982), Edelson & Malkan (1986), and Hyland & Allen (1982); *B*-band magnitudes were taken from McAlary et al. (1983); 5 GHz fluxes were taken from Ricker et al. (1978) and Unger et al. (1987).

The results from Spearman rank correlation for these extended samples are shown in Table 9. Figure 11 shows α_X versus α_{HK} and versus α_{JH} for this extended sample; Seyfert galaxies are separately identified. Table 9 shows that the inclusion of the MPC quasars does not alter the significance of the α_X versus α_{JH} correlation, but the inclusion of the luminous Seyfert galaxies weakens it; the α_X versus α_{HK} correlation becomes significant when the Seyfert galaxies are included.

The relationship between the X-ray and far-IR luminosities is illustrated in Figure 12*b*. The significance of the correlation is smaller than that between the X-ray and near-IR (see Table 7). Furthermore, both the *Ginga* and *IRAS* samples are sensitivity-limited, and we note that Sanders et al. (1989) have ascribed some previously observed correlations in luminosity-luminosity plots to an apparent relationship introduced by the redshift in flux-limited samples. Bearing in mind the limitations

TABLE 8

SIGNIFICANCE OF PARTIAL SPEARMAN RANK CORRELATION ANALYSIS

Variables Correlated	Variables Held Constant	Significance
R_L, L_X	α_X	0.02
α_X, L_X	R_L	0.11
α_X, R_L	L_X	0.92
R_L, z	α_X	0.04
α_X, z	R_L	0.21
α_X, R_L	z	0.77

TABLE 9

SIGNIFICANCE OF SPEARMAN RANK CORRELATION ANALYSIS (extended sample)

Variables Correlated	Significance: *Ginga* Sample	*Ginga* + MPC	*Ginga* + MPC + Seyferts
α_{JH}, α_X	0.06	0.06	0.13
α_{JH}, L_X	0.54	0.39	0.17
α_{JH}, R_L	0.58	0.49	0.52
α_{JH}, z	0.71	0.46	0.30
α_{JH}, α_{HK}	4×10^{-5}	1×10^{-5}	3×10^{-4}
α_{HK}, α_X	0.14	0.09	0.05
α_{HK}, L_X	0.39	0.30	0.56
α_{HK}, R_L	0.41	0.49	0.54
α_{HK}, z	0.59	0.45	0.71

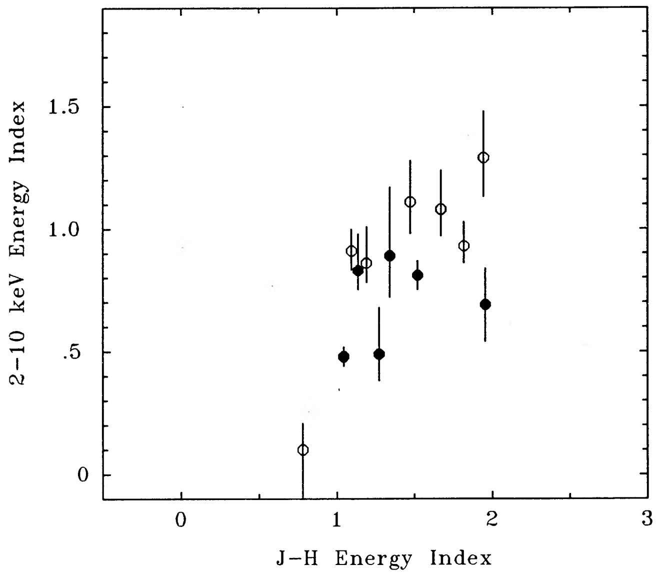

FIG. 9.—Variation of the spectral index measured by *Ginga* with the *J–H* band spectral index.

of the *Ginga* and *IRAS* samples, and also the lack of significant correlation in the X-ray and far-IR flux (Table 7 and Fig. 12*a*), this seems a plausible explanation for any correlation between the X-ray and far-IR luminosities.

Finally, Figure 13 shows the variation of α_X with the optical Fe II equivalent width. The number of quasars for which data are available is small, and no obvious correlation is visible. We note that PG 1416−129 is unusual in that it is a radio-quiet quasar, and yet does not have strong Fe II optical emission; it has been suggested that the absence of such Fe II emission could be related to flat X-ray spectra (Wilkes, Elvis, & McHardy 1987). The emission of PG 1416−129 will be discussed elsewhere. For recent discussions on the possible connection between X-ray slopes and Fe II emission see Zheng & O'Brien (1990) and Shastri et al. (1991).

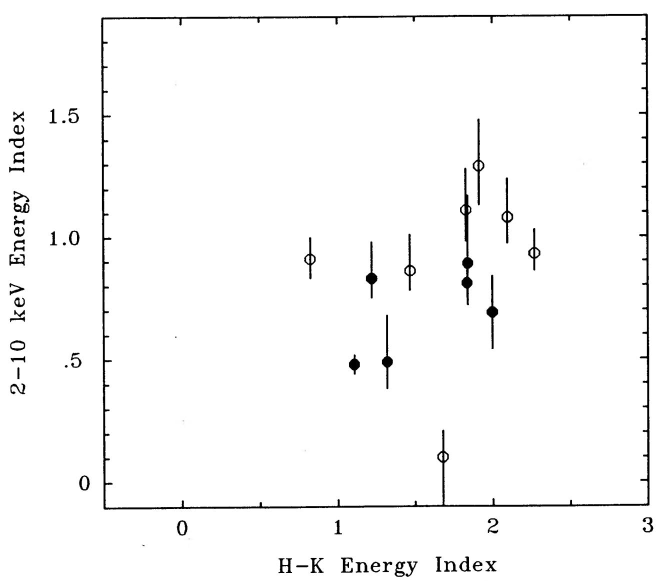

FIG. 10.—Variation of the spectral index measured by *Ginga* with the *H–K* band spectral index.

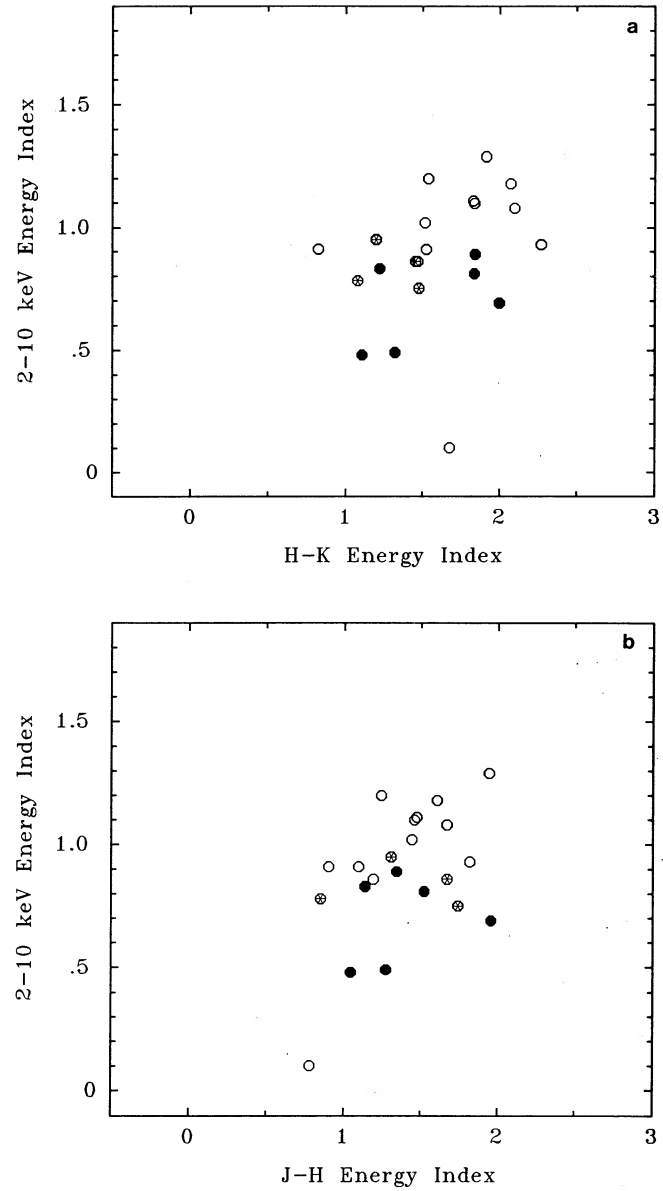

FIG. 11.—(*a*) Variation of the spectral index with the *H–K* band spectral index, for our extended sample. (*b*) Variation of the spectral index with the *J–H* band spectral index, for our extended sample. Radio-loud quasars are shown as filled circles, radio-quiet quasars as open circles, and Seyfert galaxies as circles with asterisks.

3.4. *Deviations from Power-Law Continua*

Evidence for iron emission lines has already been reported for two of the highest luminosity quasars in our ensemble, 3C 273 and E1821+643. Investigations of potential background-induced artifacts, described in Turner et al. (1990) and Kii et al. (1991), show that systematic errors could contribute at most 30% of the observed iron line intensity. The field of view containing E1821+643 may also contain a rich cluster of galaxies, but it has been shown by Kii et al. (1991) that a cluster with properties similar to those known could not contribute all of the observed line.

Table 3 shows the results of fits with and without an iron K emission line to all the observations, and shows the values of (or upper limits to) the equivalent widths derived from these fits. Five sources show a decrease in the reduced χ^2, for both local and universal background subtractions, when a narrow 6.4 keV emission line was included in the model: PKS 0637−752, PG 0804+761, Mrk 205, E1821+643, and 3C 273. However, only for E1821+643, 3C 273, and Mrk 205 is the reduction in χ^2 significant at greater than the 90% level in both cases. PKS 0637−752 shows an iron line which is significant using the "universal" background subtraction but falls below the 90% level for the "local" background. In addition to emission-line fits, Table 3 also shows both the upper limits to low-energy absorption (typically $N_H <$ several times 10^{21} cm^{-2}) and the upper limits to the depth of the iron K edge (typically $N_H < 10^{23}$ cm^{-2} for solar abundance of iron).

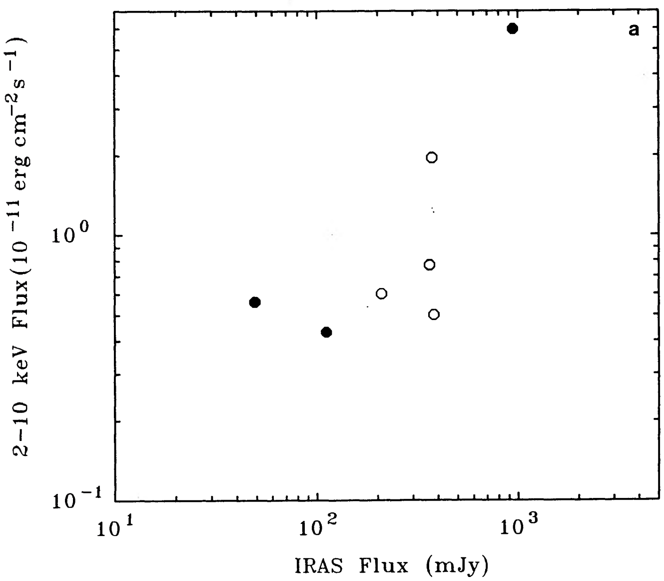

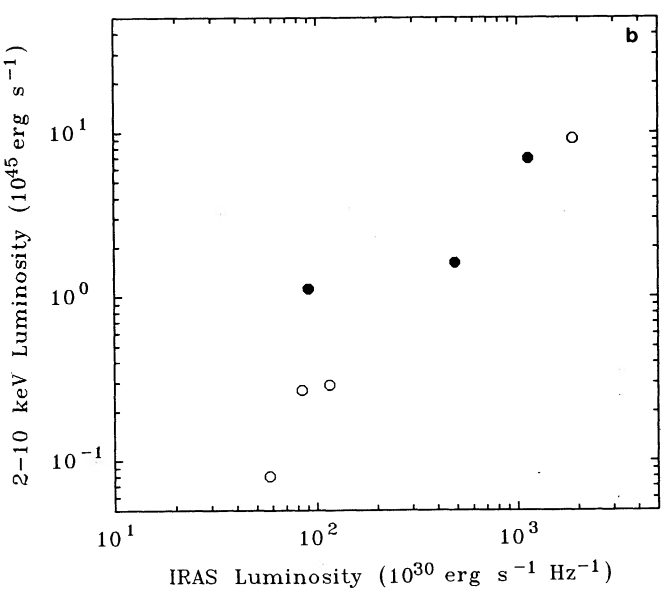

FIG. 12.—(*a*) Variation of the 2–10 keV flux (10^{-11} ergs cm^{-2} s^{-1}) measured by *Ginga* with the 25 μm flux (mJy). (*b*) Variation of the 2–10 keV luminosity (10^{45} ergs s^{-1}) measured by *Ginga* with the 25 μm luminosity (10^{30} ergs s^{-1} Hz^{-1}).

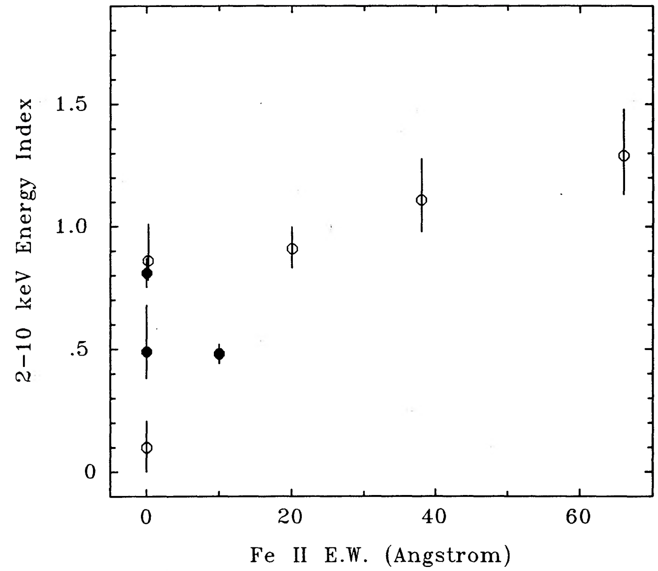

FIG. 13.—Variation of the spectral index measured by *Ginga* with the optical Fe II line equivalent width.

A number of sources are poorly fitted by a single power law. We have therefore fitted our entire sample with a number of more complex models: broken power law, two power laws, and the more specific "partial covering" and "disk reflection" models described below. Table 10 shows the values of χ^2/ν for all these models. In general we note from Table 10 that the quasars which were inadequately described by a single power law are normally well described by *any* of the more complex models, reflecting the limited resolution of the *Ginga* data.

We consider first the more empirical models: the broken power law removes the "waviness" in the residuals to the power law plus line fits to PHL 1657, PG 1416−129, and Mrk 205, although the broken power law parameters are poorly constrained. Mrk 205 and PHL 1657 are both described by power laws of $\alpha \sim 1.0$ and $\alpha \sim 0.5$ with the break at 5 keV, while PG 1416−129 is described by an $\alpha \sim 0.3$ power law which flattens above 10 keV. The two–power-law model fits the excess in the lowest channel in II Zw 136 and PG 1307+085 with a power law of $\alpha \sim 4$. However, this would imply *Einstein* fluxes of $\sim 4 \times 10^{11}$ ergs cm^{-2} s^{-1}, which are a factor of 10 higher than those observed.

Cold thermal matter in the vicinity of the quasar could explain the presence of an iron line and the departure of the continuum from a simple power-law model. Matsuoka et al. (1990) have used models where the cold material is present in the form of dense "clouds" that obscure part of the central source (partial covering models) to describe a number of *Ginga* AGN spectra. Table 11 shows the results from fitting simple partial covering models (absorption plus an emission line) to the *Ginga* data. We note that Morisawa et al. (1990) have already applied a partial covering model to the 1987 July observation of 3C 273, and report a significantly steeper slope, $\alpha = 0.69 \pm 0.05$, than that found by Turner et al. (1990), $\alpha = 0.51 \pm 0.02$, which was derived using a power law plus line

TABLE 10

COMPARISON OF χ^2/ν DERIVED FROM DIFFERENT MODELS

	POWER LAW				BROKEN POWER LAW		TWO POWER LAWS	
NAME	+ Disk Reflection	+ Partial Covering	+ Emission Line	Alone	+ Emission Line	Alone	+ Emission Line	Alone
PKS 0637−752	28/25	22/24	22/25	28/26	21/24	24/25	22/24	28/25
PG 0804+761	17/25	20/24	21/25	24/26	20/24	24/25	21/24	24/25
PKS 0837−120	14/25	16/24	16/25	16/26	12/24	12/25	16/24	16/25
PG 1211+143	15/25	18/24	19/25	20/26	15/24	17/25	17/24	18/25
PKS 1217+023	34/25	33/24	34/25	34/26	32/24	32/25	34/24	34/25
Mrk 205	30/25	23/24	41/25	51/26	20/24	27/25	23/24	27/25
3C 273	30/25	12/24	18/25	30/26	13/24	15/25	18/24	30/25
	20/25	18/24	20/25	22/26	20/24	22/25	20/24	22/25
	26/25	25/24	26/25	30/26	26/24	30/25	26/24	30/25
	20/25	15/24	17/15	20/26	17/24	20/25	17/14	20/25
	35/25	40/24	45/25	47/26	45/24	47/25	45/25	47/25
PG 1307+085	31/25	22/24	35/25	35/26	21/24	21/25	20/24	20/25
PG 1352+183	...	...	...	...	...	...	...	...
PG 1407+265	...	...	...	...	...	...	...	...
PG 1416−129	34/25	25/24	41/25	41/26	25/24	25/25	27/24	29/25
E1821+643	...	...	...	...	...	...	...	...
	35/25	17/24	18/25	36/26	15/24	22/25	18/24	36/26
II Zw 136	22/25	19/24	37/25	37/26	16/24	16/25	15/24	15/25
PHL 1657	52/25	28/24	62/25	63/25	26/24	29/25	33/24	33/25
4C 31.63	17/25	13/24	18/25	18/26	13/24	13/25	13/24	14/25

model. Our results from applying a partial covering model to the same observation are reconcilable with both Morisawa et al. and Turner et al., giving $\alpha = 0.59^{+0.08}_{-0.07}$, but the results from the other four 3C 273 observations exclude a spectral index $\alpha \sim 0.7$. Therefore, although partial covering may play a role in the emission of 3C 273, our data do not support the steep power law implied by the work of Morisawa et al.

An alternative possible geometry for cold material near the quasar center is an accretion disk. We have followed a method similar to that used by Nandra, Pounds, & Stewart (1990), and adopted by Turner et al. (1990), to analyze the spectrum of 3C 273: a power law plus "disk reflection" spectrum was fitted to the *Ginga* data, using the form of the continuum reflection given by Basko (1978). The method we used provides tighter limits than that used by Turner et al. (1990), since the iron line and edge region are included in the fit. Table 12 shows the results of fitting this power law plus reflection model to the *Ginga* data. The spectral index of the power

TABLE 11

FITS WITH POWER LAW WITH PARTIAL COVERING TO *Ginga* SAMPLE OF QUASARS AFTER "UNIVERSAL" BACKGROUND SUBTRACTION

Name	α	Covered Fraction (%)	log N_H (cm^{-2})	Line Flux (10^{-4} photons s^{-1} cm^{-2})	χ^2/ν
PKS 0637−752	$0.84^{+0.13}_{-0.09}$	17^{+83}_{-17}	$25.13^{+30.34}_{-25.13}$	$0.38^{+0.33}_{-0.35}$	22/24
PG 0804+761	$1.17^{+0.70}_{-0.06}$	52^{+48}_{-52}	$24.33^{+26.00}_{-24.33}$	$0.38^{+1.10}_{-0.38}$	20/24
PKS 0837−120	$0.87^{+0.48}_{-0.24}$	62^{+38}_{-62}	$22.04^{+26.96}_{-22.04}$	$0.00^{+0.20}_{-0.00}$	16/24
PG 1211+143	$1.18^{+0.22}_{-0.17}$	60^{+40}_{-51}	$24.40^{+25.15}_{-24.40}$	$0.37^{+407}_{-0.37}$	18/24
PKS 1217+023	$0.51^{+0.20}_{-0.14}$	9^{+91}_{-09}	$24.25^{+27.96}_{-24.25}$	$0.00^{+0.17}_{-0.00}$	33/24
Mrk 205	$1.09^{+0.27}_{-0.18}$	66^{+12}_{-19}	$24.17^{+24.44}_{-24.17}$	$0.52^{+1.90}_{-0.52}$	23/24
3C 273	$0.59^{+0.08}_{-0.07}$	14^{+03}_{-09}	$23.15^{+22.99}_{-23.10}$	$0.16^{+0.33}_{-0.16}$	12/24
	$0.56^{+0.01}_{-0.02}$	5^{+95}_{-05}	$23.51^{+25.04}_{-23.51}$	$0.07^{+0.46}_{-0.07}$	18/24
	$0.51^{+0.01}_{-0.03}$	8^{+02}_{-08}	$23.57^{+24.80}_{-23.57}$	$0.13^{+0.45}_{-0.18}$	25/24
	$0.51^{+0.02}_{-0.01}$	8^{+92}_{-08}	$23.37^{+23.51}_{-23.37}$	$0.04^{+0.50}_{-0.04}$	15/24
	$0.45^{+0.02}_{-0.02}$	10^{+01}_{-08}	$24.61^{+25.02}_{-24.61}$	$0.35^{+0.56}_{-0.35}$	40/24
PG 1307+085	$1.29^{+0.46}_{-0.42}$	71^{+17}_{-24}	$24.03^{+24.22}_{-23.73}$	$0.00^{+1.20}_{-0.00}$	22/24
PG 1352+183	...	...	...	...	...
PG 1407+265	...	...	...	...	...
PG 1416−129	$0.32^{+0.36}_{-0.20}$	66^{+16}_{-24}	$24.47^{+24.80}_{-24.21}$	$0.25^{+0.95}_{-0.25}$	25/24
E1821+643	...	...	...	...	...
	$0.99^{+0.06}_{-0.14}$	15^{+85}_{-15}	$23.05^{+23.55}_{-23.05}$	$0.48^{+0.30}_{-0.38}$	17/24
II Zw 136	$2.76^{+0.31}_{-0.41}$	76^{+12}_{-25}	$23.88^{+24.06}_{-23.58}$	$0.00^{+0.69}_{-0.00}$	19/24
PHL 1657	$0.99^{+0.15}_{-0.12}$	60^{+12}_{-16}	$24.28^{+24.43}_{-23.91}$	$0.09^{+0.70}_{-0.09}$	28/24
4C 31.63	$1.22^{+0.67}_{-0.57}$	62^{+38}_{-56}	$23.78^{+24.32}_{-23.70}$	$0.00^{+0.50}_{-0.00}$	13/24

TABLE 12

FITS WITH POWER LAW PLUS DISK REFLECTION MODEL TO *Ginga* SPECTRA AFTER "UNIVERSAL" BACKGROUND SUBTRACTION

Name	α	Reflection[a]	χ^2/ν	F[b]
PKS 0637−752	$0.90^{+0.29}_{-0.13}$	$0.00^{+1.11}_{-0.00}$	28/25	0
PG 0804+761	$1.53^{+0.78}_{-0.45}$	$2.46^{+0.54}_{-2.07}$	17/25	7.5
PKS 0837−120	$1.06^{+0.19}_{-0.36}$	$1.34^{+2.34}_{-1.34}$	14/25	3.2
PG 1211+143	$1.32^{+1.10}_{-0.26}$	$1.30^{+0.81}_{-1.30}$	15/25	6.5
PKS 1217+023	$1.50^{+0.22}_{-0.11}$	$0.00^{+0.80}_{-0.00}$	34/25	0
Mrk 205	$1.20^{+0.26}_{-0.17}$	$3.64^{+0.58}_{-1.98}$	30/25	10.7
3C 273	$0.55^{+0.05}_{-0.03}$	$0.07^{+0.21}_{-0.07}$	30/25	0
	$0.55^{+0.02}_{-0.03}$	$0.07^{+0.10}_{-0.07}$	20/25	2.3
	$0.50^{+0.04}_{-0.04}$	$0.17^{+0.18}_{-0.17}$	26/25	3.5
	$0.48^{+0.04}_{-0.03}$	$0.06^{+0.18}_{-0.06}$	20/25	0
	$0.50^{+0.04}_{-0.02}$	$0.30^{+0.19}_{-0.19}$	35/25	6.6
PG 1307+085	$1.59^{+0.48}_{-0.69}$	$4.07^{+1.82}_{-4.07}$	31/25	2.9
PG 1352+183	...	...	...	...
PG 1407+265	...	...	...	...
PG 1416−129	$0.35^{+0.17}_{-0.23}$	$1.99^{+2.55}_{-1.57}$	34/25	4.4
E1821+643	...	...	...	...
	$1.05^{+0.25}_{-0.17}$	$0.59^{+1.67}_{-0.59}$	35/25	0.7
II Zw 136	$1.85^{+0.57}_{-0.32}$	$1.88^{+0.48}_{-0.14}$	22/25	10.5
PHL 1657	$0.98^{+0.18}_{-0.12}$	$1.37^{+1.56}_{-0.94}$	52/25	4.4
4C 31.63	$0.96^{+0.66}_{-0.45}$	$2.18^{+3.02}_{-2.18}$	16/25	1.4

[a] Expressed as a ratio of the normalizations of reflected and incident components.

[b] F-statistic, $\Delta\chi^2/\chi^2_\nu$, used to measure the significance of the reduction in χ^2 by inclusion of the reflected component.

law and the size of the possible reflected term are given. The reflection is expressed as the ratio of the reflected to incident normalization, so a value of unity corresponds to a disk (subtending 2π at the source and with solar abundances) viewed face on, while a value of 0.5 corresponds to the same disk viewed at an angle of 60°.

We note that models, such as the broken power law and partial covering, have a large number of degrees of freedom and can alter the shape of the continuum; therefore, it is conceivable that they can give a perfectly acceptable fit to small continuum deviations which do not arise from the physical processes they represent. The problem is particularly relevant for *Ginga* data because systematic errors in the background subtraction can mimic small differences in the shape of the continuum: for example, an error in background subtraction can create a "hard tail" feature above 10 keV which would be well fitted by a partial covering model. Experience has shown that differences in χ^2/ν of less than $\sim 5/25$ should be treated with great caution if the phenomenological differences between the models involve components which are extended over many spectral bins; this can affect even such strong sources as 3C 273. Note, however, that this problem does not apply to additional model terms which only affect a small number of spectral bins, such as narrow emission lines: the simple power law plus line models are insensitive to differences in the background subtraction (see Tables 2 and 3).

4. DISCUSSION

Ginga has provided observations with reasonable statistical precision of the 2–10 keV spectra of 13 quasars for the first time. We are able to place constraints on parameters relevant to several current issues in X-ray astronomy based on the global properties of the present sample. In the remainder of this section we will discuss these implications of the measured quasar spectra.

4.1. *Correlations between X-Ray and Other Wave Bands*

The *Ginga* spectra reported in this paper are reasonably described by power-law models, similar to those applied to bright Seyfert I galaxies (e.g., Mushotzky 1984; Turner & Pounds 1989). There is no evidence for substantial additional thermal components in the *Ginga* range; in particular, the so-called soft excess, frequently ascribed to thermal emission from an accretion disk (e.g., E1821+643: Pravdo & Marshall 1984), has a negligible contribution in the 2–20 keV band. We can expect, therefore, that the X-ray spectra observed by *Ginga* reflect mainly the contribution of the "pure" nonthermal emission from quasars. Consequently, if the X-ray emission is part of a broad-band nonthermal continuum which underlies the emission in other wave bands, we can investigate the contribution of this continuum to those wave bands by examining correlations with the X-ray spectral parameters.

There is significant dispersion in the *Ginga* spectral indices of our sample of quasars, which makes a study of correlations with other wave bands informative. Moreover, we concur with the results of Worrall (1989), who found a broader dispersion among radio-quiet quasars than among radio-loud ones. In examining correlations with other wave bands, we have observed *differences* between radio-loud and radio-quiet quasars, and *correlations* of spectral properties among (mainly) radio-quiet quasars. In the remainder of this subsection we discuss these differences and correlations.

4.1.1. *Correlations between X-Ray and Infrared Data*

There has been considerable discussion in the literature as to whether the IR emission of quasars is thermal or nonthermal in origin. Sun & Malkan (1989) fitted the UV-IR spectra of 60 quasars and AGNs using black hole accretion disk models, and reported that the UV-IR spectra could be explained by a UV bump originating from an accretion disk together with a nonthermal power-law component. If this is so, and if, as in the SSC model (e.g., Zdziarski 1986), the nonthermal components in the IR and X-ray regions have the same origin, then we can expect the X-ray spectral parameters to depend on those in the IR region. However, Sanders et al. (1989), presenting the multi-frequency spectra of 109 bright quasars from the PG survey, concluded that nonthermal emission dominates the IR band only in a few cases, such as the extreme (highly polarized) flares seen in 3C 273. In the majority of cases they interpreted the IR emission in terms of reradiation from dust.

If a link between the IR spectral indices and X-ray spectral parameters could be established, this might indicate the presence of a significant nonthermal component in the IR emission. The X-ray spectral slopes reported here are significantly flatter than those near 3 μm (Figs. 9 and 10), so the near-IR and X-ray emission in the majority of our sample cannot, therefore, be interpreted as part of a unified power law joining the IR and X-ray bands. The correlation between near-IR spectral index, α_{JH}, and the X-ray spectral index is of limited statistical significance (see § 3.3); it may, however, support the connection between the soft X-ray and near-IR band which has previously been suggested by a number of authors (see below). It may be significant that the observed correlation between the IR and the *Ginga* X-ray spectral indices is apparent mainly in the radio-quiet objects. The addition of the *Einstein* monitor proportional counter (MPC) quasars and the *EXOSAT* Seyfert galaxies to our sample is inconclusive: the significance of the α_X versus α_{JH} correlation declines, while that of the α_X versus α_{HK} correlation increases slightly. We have argued elsewhere that Seyfert galaxies may have different properties in the 2–10 keV band from quasars; their inclusion may not be valid, particularly if they have only a narrow distribution in α_X.

We have also searched for correlations in the X-ray and IR flux-flux and luminosity-luminosity plots. While there is no evidence for a correlation between the X-ray and far-IR luminosities, there is a statistically significant, and approximately linear, correlation between the X-ray luminosities reported here and the corresponding near-IR luminosities (see Fig. 8*b* and Table 7). However, because our sample is small and heterogeneous, it is impossible to assess whether the X-ray and near-IR luminosities are strongly correlated, as might be expected if the X-ray and near-IR have closely related emission mechanisms.

In spite of the possibility of confusion due to the soft X-ray excess, a large number of authors have previously investigated the relationship between the soft X-ray and IR luminosities of AGNs. There is general agreement that no correlation exists between the far-IR and the soft X-ray bands (Neugebauer et al. 1986; Carleton et al. 1987). However, the situation between the near-IR and soft X-ray is far more complex. The claim that the 3 μm and 2 keV luminosities are closely, and approximately linearly, related has been made by Malkan (1984) and also by Elvis et al. (1986). A similar tight correlation between the 3–10 μm luminosities and soft X-ray luminosity has been reported by Carleton et al. (1987). Most recently, Mushotzky & Wandel (1989) reported that the soft X-ray luminosity has a flatter dependence on the 750 nm luminosity than on the 420 nm luminosity, and suggested that this supported a nonthermal origin for the near-IR emission. However, in contrast to the above, McAlary & Rieke (1988), after considering the (weak) correlation between the soft X-ray and 3 μm fluxes for the PG quasars, conclude that while there might be a universal underlying spectrum, many objects might have X-ray absorption or a substantial IR excess superposed on this. Similarly, Sanders et al. (1989) ascribe the previously observed strong correlations to the apparent relationship in luminosity-luminosity plots of flux-limited samples introduced by the redshift, and conclude that there is no reason to invoke a common mechanism in the production of the X-ray to IR continuum of the majority of AGNs.

In conclusion, the evidence (albeit at only $\sim$95% significance) of a correlation between the X-ray spectral index, α_X, and the near-IR spectral index, α_{JH}, is of greatest interest, since such a relationship may indicate related emission mechanisms for these regions. The correlation observed between the near-IR and X-ray luminosities could be used to support the same hypothesis. However, we cannot determine the true strength of this latter correlation, and it is plausible that a weak correlation could arise simply because the X-ray and near-IR luminosity are independently related to some third parameter, such as the accretion rate. Finally, *Ginga* results are consistent with the previously observed lack of connection between the X-ray and far-IR bands.

4.1.2. *Correlations between X-Ray and Radio Data*

The possibility of a correlation in the *Ginga* data between α and radio-loudness is of great interest. Its presence would strongly support the view that the correlation observed in the soft X-ray (Wilkes & Elvis 1987; Canizares & White 1989; Worrall 1989) is independent of any soft excess ("ultra-soft," in Wilkes & Elvis) and arises from the underlying (power-law) continuum. This would enable constraints to be placed on current models.

The five steepest spectrum quasars in our sample are radio-quiet, suggesting that quasars with steep spectra are radio-quiet (although the converse, that radio-quiet quasars have steep spectra, is not universally true, e.g., PG 1416−129). The Kolmogorov–Smirnov test gives a probability of only 7% that the distributions of α observed for radio-loud and radio-quiet quasars are drawn from the same population. However, as discussed in § 3.3, luminosity and redshift, in our sample, are not independent of the radio-loudness: all our low-luminosity quasars are radio-quiet and have relatively low redshifts, while our high-luminosity quasars, except for E1821+643, are all radio-loud objects at high redshifts. Consequently, a partial Spearman rank analysis cannot determine which of these three quantities is fundamentally related to the spectral slope. However, we note the close similarity of our data to those of Wilkes & Elvis (1987), who found trends in their IPC data linking α with R_L, luminosity, and redshift. They had sufficient overlap between the range of luminosities covered by radio-quiet and radio-loud quasars to determine, using partial Spearman rank correlation analysis, that the fundamental correlation, after allowing for the interdependence of the variables, was between α and R_L. This implies that the fundamental relation in our sample may also be between R_L and α.

Reconciliation of the observed relationship between α and R_L in the *Einstein* data, and the tightly grouped, and flatter, spectra of the radio-quiet AGNs (mainly Seyfert galaxies) observed by *HEAO 1* A-2, led Wilkes & Elvis (1987) to argue that quasar spectra in the *Einstein* band are comprised of up to three components: the soft excess component which is an established feature of at least some AGNs (e.g., Arnaud et al. 1985; Pounds et al. 1986); a steep component, $\alpha \sim 1.0$; and a flat component, $\alpha \sim 0.5$, which is linked to the radio emission. They argued that the progressive dominance of the flat component with increasing energy was responsible for the flatter *HEAO 1* A-2 spectra.

The *Ginga* results on the spectra of radio-quiet quasars, in the same energy band as *HEAO 1* A-2, agree with the *Einstein* data rather than with the *HEAO 1* A-2 data. For the Wilkes & Elvis radio-quiet quasars $\bar{\alpha} = 0.98 \pm 0.14$, while for the *HEAO 1* A-2 radio-quiet AGNs $\bar{\alpha} = 0.66 \pm 0.14$; however, for the *Ginga* radio-quiet quasars $\bar{\alpha} = 1.03 \pm 0.16$, i.e., identical to the *Einstein* result. Furthermore, the *Ginga* and *Einstein* measurements of the spectral slopes of individual quasars seem to be correlated, and the two sets of results are compatible with only two, reasonable, exceptions (see § 3.2). Consequently, there is less reason for requiring a "two-component" model of the X-ray continuum. However, our data do not exclude the possibility that quasars have a separate flat spectral component, linked to their radio emission: the upper limit to a flat component in the spectrum of E1821+643, the brightest radio-quiet quasar in the *Ginga* sample, is $\sim$20%, with less stringent limits for the fainter objects.

It is probable that the differences found between the *Einstein* and *HEAO 1* A-2 data are due to the very different samples of AGNs contained in them, and are not due to the difference in the observed energy bands. In this context we note that recent observations of AGNs using *Ginga* have suggested that Seyfert galaxies, which dominate the *HEAO 1* A-2 sample, have spectra in the 2–10 keV band which are comprised of a steep power law, $\bar{\alpha} \sim 1.0$, and a "reflected" component, which together may give the appearance of a spectrum with a slope of 0.7, in an instrument with slightly worse energy resolution than *Ginga* (Pounds et al. 1990; Matsuoka et al. 1990). This does not appear to be the case for some quasars, where a pure power law is a better fit to the data (see § 4.3), and may well be the true origin of the discrepancy between the *Einstein* and *HEAO 1* A-2 results. We also note the contrast between Seyfert galaxy spectra, where the power laws observed by *Einstein* are steeper than those observed by *HEAO 1* A-2 (Kruper, Urry, & Canizares 1990), and quasar spectra, where the *Ginga* and *Einstein* values are compatible. The steepening in the *Einstein* Seyfert galaxy spectra could, at least in part, be explained by the presence of a soft excess. Conversely, Wilkes & Elvis argue that the soft excess in quasars is at low enough energies not to affect the derived power-law fit, and also quasars generally have weaker soft excesses than Seyfert galaxies (Masnou et al. 1991; Comastri et al. 1992; Saxton et al. 1991).

We conclude that our data support a connection between the X-ray power-law continuum and radio emission of quasars. There is no evidence in our data to suggest that observed quasar spectra arise from a mixture of $\alpha \sim 0.5$ and $\alpha \sim 1.0$ power laws. Instead, our data are compatible with the X-ray spectra of quasars being dominated by a single power law, throughout the *Ginga* and *Einstein* bands. Therefore, although the limits are not sufficiently stringent to exclude the existence of a flat component in the radio-quiet quasars, there is no reason to favor models which predict it. As more *Ginga* data become available, we should be able to investigate further the connection between α and R_L.

4.2. *Deviations from the Power-Law Continuum*

A number of the quasars observed by *Ginga* are not well described by simple power-law spectra, and require the addition of extra components. Deviations from a power-law continuum, ascribed to iron K emission lines, have already been reported in the *Ginga* spectra of 3C 273 (Turner et al. 1990) and E1821+643 (Kii et al. 1991). Similar iron K emission lines with equivalent widths of 100–200 eV have been reported from *EXOSAT* and *Ginga* observations of a number of Seyfert galaxies, and appear to be a common feature of such objects. It is plausible that the line emission features in Seyfert galaxies and quasars have similar origins, reflecting common emission mechanisms among different classes of AGNs. If so, we would expect iron lines with equivalent widths ~ 100 eV to be a common feature of quasar spectra. Our data are compatible with this hypothesis: the addition of a narrow emission line at 6.4 keV significantly improves the fit to Mrk 205 and the previously reported cases of 3C 273 (Turner et al. 1990) and E1821+643 (Kii et al. 1991); PKS 0637−752 shows marginal evidence for an iron emission line; and the remainder of the objects have upper limits in the range 140–600 eV.

Iron lines can originate from the thermal emission of hot material or fluorescence from either hot or cold material. Turner et al. (1990) and Kii et al. (1991) note that there is no strong evidence that the iron lines in 3C 273 and E1821+643 have a thermal origin, and we cannot add further constraints to thermal emission using our data.

The iron K emission lines in Seyfert galaxies have been attributed to fluorescence of material illuminated by radiation from the central core (e.g., Nandra et al. 1990; Matsuoka et al. 1990). In general, assuming that the matter is cold material, distributed isotropically around the central core, results in an expected low-energy absorption which exceeds that actually measured. The data from our quasars are similar: none of them show evidence for cold material uniformly covering the central source in the line of sight. The limits are relatively stringent, being typically $N_H < 1 \times 10^{22}$ cm^{-2} for the fainter quasars. The amount of material necessary to produce a line of ~ 100 eV equivalent width is $\sim 1 \times 10^{23}$ cm^{-1} (Inoue 1985). Thus fluorescence in cold material in the line of sight cannot be the cause of the deviations from the simple power law that we have observed. However, alternative geometries or the assumption of a high ionization parameter could of course explain this.

One suggestion for Seyfert galaxies is that cold material is present in the form of dense "clouds" that obscure part of the central source (e.g., Matsuoka et al. 1990); the iron line arises from fluorescence, and a high-energy excess (or "hard tail") arises from transmission through the "partial covering." We have fitted a partial-covering model to all of our quasar sample, and the results are presented in Table 11. Unlike the power law plus line model, this model gives formally acceptable values of χ^2/ν for all of our sample of quasars. Therefore, cold material in the form of clouds partly obscuring the central source of quasars is a possible source of the features seen in the spectra of the *Ginga* quasar sample. However, we note the concerns about the class of model expressed in § 3.4, and also that empirical two-component models give an adequate fit. We conclude, therefore, that it would be premature to assume that this geometry is necessarily correct.

Compton reflection and fluorescence from material which is present in the form of an accretion disk is another model which has been used (Nandra et al. 1990) to explain the spectra of Seyfert galaxies. These models show that for a face-on disk illuminated by the continuum the effective iron line equivalent width would be ~ 150 eV (Basko 1978; Nandra et al. 1990; George & Fabian 1991) and that this equivalent width decreases as the inclination rises. Section 3.4 has given the results obtained from fitting a simple disk reflection model to the data. This model gives improvements, compared with the power law plus line model, of >90% significance according to the *F*-test, to fits to the spectra of PHL 1657, PG 1416−129, Mrk 205, and II Zw 136, although we accept that the *F*-test may overestimate the significance of this improvement (see § 3.4). It is instructive to examine these fits for evidence of differences between high- and low-luminosity objects. First, we note that the two objects which show the most significant *reduction* in χ^2 when changing from power law plus line models to power law plus disk reflection models are the two lowest luminosity and lowest redshift objects, Mrk 205 and II Zw 136. Second, the disk reflection fit to the higher luminosity PHL 1657 data is formally unacceptable and the value of the reduced χ^2 is higher than that of the partial-covering model. Finally, the three objects with the highest luminosities, PKS 0637−752, E1821+643, and 3C 273, all show *increases* in reduced χ^2 when changing from power law plus line models to power law plus disk reflection models. In the case of E1821+643 this might be explained by the presence of emission from the cluster surrounding this quasar, but no such simple explanation is available for 3C 273.

The above arguments show that the disk reflection model not only successfully describes the spectra of Seyfert I galaxies but also is compatible with quasars with modest luminosities, most noticeably Mrk 205; however, it is not as good a fit to the higher luminosity quasars in our sample. This may indicate a difference between the X-ray emission of high- and low-luminosity AGNs. Such a difference could be due to beaming: 3C 273, for example, is known to be superluminous, and therefore some beaming must be present. This may account for the small iron K equivalent width in 3C 273, and may also contribute to the other observed differences. We note that iron K emission lines have not been detected from BL Lac objects and OVV quasars, with typical upper limits to their equivalent width of 100–600 eV (Ohashi et al. 1989). In particular, on 1989 July 3 the OVV quasar 3C 279 had an X-ray flux of 6×10^{-11} ergs cm^{-2} s^{-1} in the 2–10 keV band, which is as bright as 3C 273. However, no iron emission was detected, and the upper limit to the equivalent width was 20 eV (Makino et al. 1989). We believe that the continuum emission from OVV quasars and BL Lac objects is large, because of the effect of beaming, and that the iron line emission is relatively faint because it is not similarly enhanced.

In conclusion we reiterate the following. Three of our quasars show significant deviations from power-law models; the remainder show evidence of lower significance, or have upper limits compatible with iron lines with equivalent widths of ~ 100 eV. All of our quasars can be adequately described by a "partial covering plus emission line" model, although it would be premature to conclude that partial covering of the central source by cold material is the origin of the observed deviations from a simple power law. The Seyfert galaxies and the lower luminosity quasars are well described by a power law plus disk reflection model, while the higher luminosity sources may not be; this suggests a difference between low- and high-luminosity AGNs.

4.3. *Implications for the CXB*

The contribution of AGNs to the CXB has been estimated by several authors (e.g., Schmidt & Green 1986; Giacconi & Zamorani 1987), and a significant contribution ($\sim 30\%$) of low-luminosity AGNs ($L_X < 10^{44}$ ergs s^{-1}) has been suggested. A direct study of the X-ray luminosity function of AGNs and its evolution has been carried out based on the *Einstein* Extended Medium-Sensitivity Survey (EMSS) sample (Maccacaro et al. 1991). The measured local luminosity function flattens at $L_X < 10^{43.3}$ ergs s^{-1}, and evidence for significant evolution at $z \leq 0.4$ is found. The total AGN contribution to the CXB at 2 keV is about 40%, of which about 60% comes from objects with de-evolved luminosities between 10^{43} and 10^{44} ergs s^{-1}. A third of the AGN contribution is due to objects in the redshift range 1–2. Considering evolution, the luminosity at $z = 1$–2 is 8–16 times higher than the de-evolved value; therefore the important range of AGN luminosity would be from 10^{44} to several times 10^{45} ergs s^{-1}. This is the range studied in the present observations.

The log N–log S relationship, measured in the 2–10 keV range, indicates that the source counts in this band exceed the EMSS result by a factor of 3 (Boldt 1988; Warwick & Stewart 1989; Hayashida 1990). At the same time, based on the measured spectrum of the CXB fluctuations, Warwick & Stewart (1989) and Hayashida (1990) have shown that the sources at $F_X \sim 10^{-12}$ ergs cm^{-2} s^{-1} in the 2–10 keV band are mostly AGNs. If one takes the higher source counts in the 2–10 keV band at face value, an almost 100% contribution of AGNs to the CXB would be implied. This enhances the importance of the quasar survey observations with *Ginga*.

We have reported on the spectral indices of the AGNs over the luminosity range 10^{44}–10^{46} ergs s^{-1}, a range which, as argued above, has relevance to the potential contribution of AGNs to the CXB. It is well known that the lower luminosity AGNs have a mean spectral index $\bar{\alpha} \sim 0.7$ (Mushotzky 1984; Turner & Pounds 1989), which is too steep for such objects to contribute significantly to the much flatter CXB without significant spectral evolution—thus giving rise to the so-called spectral paradox. Our results show that this is also true for the higher luminosity objects. Indeed, the mean spectral index for quasars ($\bar{\alpha} \sim 0.81$) is, perhaps, larger than that for Seyfert galaxies, making it even harder to explain the measured index of the CXB ($\alpha = 0.4$) in terms of quasars as opposed to Seyfert galaxies. Assuming that quasars having such steep X-ray spectra account for 50% of the CXB, the remaining spectrum after subtracting the quasar contribution should have $\alpha \sim 0$ in the 2–20 keV band. None of the known types of X-ray sources have such flat spectra, and, although we note that the spectrum of PG 1416+129 reported in this paper is sufficiently flat, we do not know enough about this object to regard it as a potential prototype for the unknown CXB sources.

Although the sample is still small, the present observations have clearly indicated that, if our measured spectra are representative of quasar spectra at higher redshifts, it is not possible to explain all of the CXB with quasars. Several possibilities have been studied in an attempt to solve this problem. Among them, the recent finding of the iron-edge structure in the spectra of Seyfert galaxies (Pounds et al. 1990; Matsuoka et al. 1990) has suggested the possibility that the necessary flat spectrum may be produced by absorption (Fabian et al. 1990; Morisawa et al. 1990). Combinations of absorbed or reflected spectra at different redshifts can indeed reproduce the observed spectrum of the CXB in the energy range 1–100 keV. However, none of the quasars in the present sample (excluding perhaps the nearby object Mrk 205) reveal evidence for an iron-edge feature. In particular, stringent upper limits are derived for the two bright objects, 3C 273 and E1821+643 (see also Turner et al. 1990; Kii et al. 1991). In their lack of iron-edge features the continua of these two quasars differ significantly from those of Seyfert galaxies. We note that none of the quasars in the Wilkes & Elvis (1987) sample indicate low-energy absorption, although both the Wilkes & Elvis and the *Ginga* samples are chosen from quasars with a large soft X-ray flux, which could introduce selection effects (as discussed in § 2). These results do not support the suggestion that absorbed AGN spectra are the major source of the flat spectrum of the CXB.

Let us quickly explore the remaining possibilities. The present sample of quasars is biased to high-luminosity objects. Recent studies suggest the presence of beaming in a substantial number of quasars (Browne & Murphy 1987; Barthel 1989). Discovery of a 6 minute X-ray flare from a non–OVV quasar, PKS 0558−504 (Remillard et al. 1991), directly indicates X-ray beaming in this object. If the X-ray emission of the quasars studied so far, in particular those in the present sample, is beamed toward us, the existence of a large population of misbeamed quasars is naturally implied. These low-luminosity objects may possess the necessary flat spectral slope, possibly due to absorption, to account for the CXB. However, the study of Maccacaro et al. (1991) indicates that 60% of the CXB at 2 keV is not due to AGNs. This implies a substantial contribution from an unknown class of objects, even if one considers the emission of clusters and normal galaxies. Although *ROSAT* may identify contributors to the 2 keV background, the complete solution to the origin of the CXB may have to await future survey observations with high-sensitivity X-ray missions.

5. CONCLUSIONS

The observations of quasars with *Ginga* have led to a number of significant new facts emerging on their X-ray spectra.

There is evidence in our data for a correlation between radio-loudness (or 2–10 keV luminosity) and X-ray spectral index, which supports the spectral index–radio-loudness correlation found in the lower energy IPC data by Wilkes & Elvis (1987); however, our data show no evidence for flattening of the slope between the *Einstein* and *Ginga* bands, and consequently there is no support for the suggestion that observed quasar spectra arise from a mixture of $\alpha \sim 0.5$ and $\alpha \sim 1.0$ power-law components. Our data are equally consistent with there being two populations of quasars, radio-loud and radio-quiet, each having spectra dominated by a single power law.

There is some evidence for a link between near-IR and X-ray emission. In particular, the link between the near-IR spectral slope and the X-ray spectral slope, at $\sim 95\%$ significance, provides some support to models in which the X-ray and IR emission arise from related processes. However, there is an absence of corroborative evidence from other samples.

At least three of our quasars show significant deviations from simple power-law models, and our data are compatible with all quasars having iron lines with equivalent widths of ~ 100 eV. The spectra of the lower luminosity quasars in our sample are compatible with the power law plus disk reflection models, found to fit spectra from Seyfert I galaxies. These models are not such a good fit to the higher luminosity sources; this may indicate a difference between the X-ray properties of low- and high-luminosity AGNs.

While the distribution of spectral indices in our sample is rather broad, with at least two of the quasars, 3C 273 and PG 1416−129, having flat spectra, the mean spectral index ($\bar{\alpha} = 0.81$) is steeper than the spectrum of the CXB, confirming the "spectral paradox" in the discrete-source explanation of the CXB. If the majority of quasars observed by us are beamed, the implied population of misbeamed quasars could, perhaps by means of absorption, produce a spectrum which matches that of the CXB.

The authors would like to thank all the members of the *Ginga* team, who have provided support during the course of the *Ginga* observations and subsequent analysis; Paul Nandra for valuable discussions during the course of this work; and Belinda Wilkes for supplying some unpublished *Einstein* results. We are grateful for some helpful comments by the referee. G. C. S. acknowledges the support of the SERC in the form of an advanced fellowship.

REFERENCES

Angel, J. R. P., & Stockman, H. S. 1980, ARA&A, 18, 321
Arnaud, K. A., et al. 1985, MNRAS, 217, 105
Barthel, P. D. 1989, ApJ, 336, 606
Basko, M. M. 1978, ApJ, 223, 268
Berriman, G. 1990, ApJ, 354, 148
Bregman, J. N., et al. 1986, ApJ, 301, 708
Browne, I. W. A., & Murphy, D. W. 1987, MNRAS, 226, 601
Boldt, E. 1988, in Physics of Neutron Stars and Black Holes, ed. Y. Tanaka (Tokyo: Universal Academy Press), 333
Canizares, C. R., & White, J. L. 1989, ApJ, 339, 27
Carleton, N. P., Elvis, M., Fabbiano, G., Willner, S. P., Lawrence, A., & Ward, M. 1987, ApJ, 318, 595
Comastri, A., Setti, G., Zamorani, G., Elvis, M., Giommi, P., Wilkes, B. J., & McDowell, J. C. 1992, ApJ, 384, 62
Courvoisier, T. J.-L., et al. 1990, A&A, 234, 73
Edelson, R. A., & Malkan, M. A. 1986, ApJ, 308, 59
Elvis, M., Green, R. F., Bechtold, J., Schmidt, M., Neugebauer, G., Soifer, B. T., Matthews, K., & Fabbiano, G. 1986, ApJ, 310, 291
Elvis, M., Lockwood, F. J., & Wilkes, B. J. 1989, AJ, 97, 777
Fabbiano, G., Gioia, I. M., & Trinchieri, G. 1988, ApJ, 324, 749
Fabian, A. C. 1988, in Supermassive Black Holes, ed. M. Kafatos (Cambridge: Cambridge Univ. Press), 234
Fabian, A. C., George, I. M., Miyoshi, S., & Rees, M. J. 1990, MNRAS, 242, 14
George, I. M., & Fabian, A. C. 1991, MNRAS, 249, 352
Giacconi, R., & Zamorani, G. 1987, ApJ, 313, 20
Hayashida, K. 1990, Ph.D. thesis, Univ. Tokyo
Hayashida, K., et al. 1989, PASJ, 41, 373
Hewitt, A., & Burbidge, G. 1987, ApJS, 63, 1
Hyland, H. R., & Allen, D. A. 1982, MNRAS, 199, 943
Inoue, H. 1985, Space Sci. Rev., 40, 317
Johnson, H. L. 1966, ARA&A, 4, 193
Jones, T. W., O'Dell, S. L., & Stein, W. A. 1974, ApJ, 188, 353
Kellermann, K. I., Sramek, R., Schmidt, M., Shaffer, D. B., & Green, R. 1989, AJ, 98, 1195
Kembhavi, A., Feigelson, E. D., & Singh, K. P. 1986, MNRAS, 220, 51
Kii, T., et al. 1991, ApJ, 367, 455
Kolman, M., Halpern, J. P., Shrader, C. R., & Filippenko, A. V. 1991, ApJ, 373, 57
Kruper, J. S., Urry, C. M., & Canizares, C. R. 1990, ApJS, 74, 347
Maccacaro, T., Della Ceca, R. D., Gioia, I. M., Morris, S. L., Stocke, J. T., & Wolter, A. 1991, ApJ, 374, 117
Macklin, J. T. 1982, MNRAS, 199, 1119
Makino, F., & the ASTRO-C Team. 1987, Astrophys. Lett. Comm., 25, 223
Makino, F., et al. 1989, ApJ, 347, L9
Malkan, M. A. 1984, in X-Ray and UV Emission from Active Galactic Nuclei, ed. W. Brinkmann & S. Trumper (Max Planck Rep., No. 184), 121
Masnou, J.-L., Wilkes, B. J., Elvis, M., McDowell, J. C., & Arnaud, K. A. 1991, A&AS, in press
Matsuoka, M., Ikegami, T., Inoue, H., & Koyama, K. 1986, PASJ, 38, 285
Matsuoka, M., Piro, L., Yamauchi, M., & Murakami, T. 1990, ApJ, 361, 440
McAlary, C. W., McLaren, R. A., McGonegal, R. J., & Maza, J. 1983, ApJ, 52, 341
McAlary, C. W., & Rieke, G. H. 1988, ApJ, 333, 1
McHardy, I. M. 1989, in Proc. 23d ESLAB Symp. on Two Topics in X-Ray Astronomy (ESA SP-296; Noordwijk: ESA), 1111
Miley, G. K., & Hartsuijker, A. P. 1978, A&AS, 34, 129
Morisawa, K., Matsuoka, M., Takahara, F., & Piro, L. 1990, A&A, 236, 299
Mushotzky, R. F. 1984, Adv. Space Res., 3 (Nos. 10–12), 157
Mushotzky, R. F., & Wandel, A. 1989, ApJ, 339, 674
Nandra, K., Pounds, K. A., & Stewart, G. C. 1990, MNRAS, 242, 660
Neff, S. G., & Browne, R. L. 1984, AJ, 89, 195
Neugebauer, G., Green, R. F., Matthews, K., Schmidt, M., Soifer, B. T., & Bennett, J. 1987, ApJ, 63, 615
Neugebauer, G., Miley, G. K., Soifer, B. T., & Clegg, P. E. 1986, ApJ, 308, 815
Neugebauer, G., Oke, J. B., Becklin, E. E., & Matthews, K. 1979, ApJ, 230, 79
Ohashi, T., et al. 1989, in Proc. 23d ESLAB Symp. on Two Topics in X-Ray Astronomy (ESA SP-296; Noordwijk: ESA), 837
Perley, R. A. 1982, AJ, 87, 859
Petre, R., Mushotzky, R. F., Krolik, J. H., & Holt, S. S. 1984, ApJ, 280, 499
Piro, L., Matsuoka, M., & Yamauchi, M. 1989, in Proc. 23d ESLAB Symp. on Two Topics in X-Ray Astronomy (ESA SP-296; Noordwijk: ESA), 819
Pounds, K. A. 1989, in Proc. 23d ESLAB Symp. on Two Topics in X-Ray Astronomy (ESA SP-296; Noordwijk: ESA), 753
Pounds, K. A., Nandra, K., Stewart, G. C., George, I. M., & Fabian, A. C. 1990, Nature, 344, 132
Pounds, K. A., Nandra, K., Stewart, G. C., & Leighly, K. 1989, MNRAS, 240, 769
Pounds, K. A., Stanger, V. J., Turner, T. J., King, A. R., & Czerny, B. 1986, MNRAS, 224, 443
Pravdo, S. H., & Marshall, F. E. 1984, ApJ, 281, 570
Press, W. H., Flannery, B. P., Teukolsky, S. A., & Vetterling, W. T. 1986, Numerical Recipes (Cambridge: Cambridge Univ. Press), 488
Remillard, R. A., Grossan, B., Bradt, H. V., Ohashi, T., Hayashida, K., Makino, F., & Tanaka, Y. 1991, Nature, 350, 589
Ricker, G. R., et al. 1978, Nature, 271, 35
Sanders, D. B., Phinney, E. S., Neugebauer, G., Soifer, B. T., & Matthews, K. 1989, ApJ, 347, 29
Savage, A. 1976, MNRAS, 174, 259
Saxton, R. D., Turner, M. J. L., Williams, O. R., Stewart, G. C., Ohashi, T., & Kii, T. 1991, MNRAS, submitted
Schmidt, M., & Green, R. F. 1983, ApJ, 269, 352
———. 1986, ApJ, 68

Shastri, P., Wilkes, B. J., Elvis, M., & McDowell, J. C. 1991, in Proc. Heidelberg Conf. on the Physics of AGNs, in press
Shimmins, A. J., & Bolton, J. G. 1972, Australian J. Phys. Astrophys. Suppl., 32, 1
Stark, A. A., Heiles, C., Bally, J., & Linke, R. 1984, Bell Laboratories, privately distributed magnetic tape
Sulentic, J. W., & Arp, H. C. 1987, ApJ, 319, 693
Sun, W.-H., & Malkan, M. A. 1989, ApJ, 346, 68
Turner, M. J. L., et al. 1989, PASJ, 41, 345
Turner, M. J. L., et al. 1990, MNRAS, 244, 310
Turner, T. J., & Pounds, K. A. 1989, MNRAS, 240, 833
Unger, S. W., Lawrence, A., Wilson, A. S., Elvis, M., & Wright, A. E. 1987, MNRAS, 228, 521
Véron-Cetty, M.-P., & Véron, P. 1984, ESO Sci. Rep., No. 1, p. 1
Ward, M., Allan, D. A., Wilson, A. S., Smith, M. G., & Wright, A. E. 1982, MNRAS, 199, 953
Warwick, R. S., & Stewart, G. C. 1989, in Proc. 23d ESLAB Symp. on Two Topics in X-Ray Astronomy (ESA SP-296; Noordwijk: ESA), 727
Wilkes, B. J., & Elvis, M. 1987, ApJ, 323, 243
Wilkes, B. J., Elvis, M., & McHardy, I. 1987, ApJ, 321, L23
Wilkes, B. J., Masnou, J.-L., Elvis, M., McDowell, J., & Arnaud, K. 1989, in Proc. 23d ESLAB Symp. on Two Topics in X-Ray Astronomy (ESA SP-296; Noordwijk: ESA), 1081
Worrall, D. M. 1988, in Active Galactic Nuclei, ed. H. R. Miller & P. J. Wiita (Heidelberg: Springer-Verlag), 248
———. 1989, in Proc. 23d ESLAB Symp. on Two Topics in X-Ray Astronomy (ESA SP-296; Noordwijk: ESA), 719
Worrall, D. M., & Wilkes, B. J. 1990, ApJ, 360, 396
Zamorani, G., et al. 1981, ApJ, 245, 357
Zdziarski, A. A. 1986, ApJ, 305, 45
Zensus, J. A., Porcas, R. W., & Pauliny-Toth, I. I. K. 1984, A&A, 133, 27
Zheng, W., & O'Brien, P. T. 1990, ApJ, 353, 443